Thermo-tectonic history of the Issyk-Kul basement (Kyrgyz Northern Tien Shan, Central Asia)

Article *in* Gondwana Research · January 2012

DOI: 10.1016/j.gr.2012.06.014

6 authors, including:

Johan De Grave
Ghent University
99 PUBLICATIONS **1,570** CITATIONS
SEE PROFILE

Stijn Glorie
University of Adelaide
89 PUBLICATIONS **1,108** CITATIONS
SEE PROFILE

M.M. Buslov
Sobolev Institute of Geology and Mineralogy
180 PUBLICATIONS **4,659** CITATIONS
SEE PROFILE

Daniel F. Stockli
University of Texas at Austin
461 PUBLICATIONS **7,159** CITATIONS
SEE PROFILE

Gondwana Research 23 (2013) 998–1020

Contents lists available at SciVerse ScienceDirect

Gondwana Research

journal homepage: www.elsevier.com/locate/gr

Thermo-tectonic history of the Issyk-Kul basement (Kyrgyz Northern Tien Shan, Central Asia)

Johan De Grave [a,*], Stijn Glorie [a], Mikhail M. Buslov [b], Daniel F. Stockli [c,d], Michael O. McWilliams [e,f], Vladislav Yu. Batalev [g], Peter Van den haute [a]

[a] Department of Mineralogy & Petrology, Ghent University, Ghent, Belgium
[b] Institute of Geology & Mineralogy, Siberian Branch, Russian Academy of Sciences, Novosibirsk, Russia
[c] Department of Geology, Kansas State University, Lawrence, KS, USA
[d] Jackson School of Geosciences, University of Texas, Austin, TX, USA
[e] Department of Geological & Environmental Sciences, Stanford University, Stanford, CA, USA
[f] CSIRO Earth Science and Resource Engineering Division, Perth, Australia
[g] International Research Station, Russian Academy of Sciences, Bishkek, Kyrgyzstan

ARTICLE INFO

Article history:
Received 20 December 2011
Received in revised form 13 June 2012
Accepted 13 June 2012
Available online 11 July 2012

Handling Editor: W.J. Xiao

Keywords:
Kyrgyz Tien Shan
Issyk-Kul Basin
Thermochronology
Zircon U/Pb
Tectonics

ABSTRACT

Lake Issyk-Kul occupies a large Late Mesozoic–Cenozoic intramontane basin between the mountain ranges of the Northern Kyrgyz Tien Shan. These ranges are often composed of granitoid basement that forms part of a complex mosaic assemblage of microcontinents and volcanic arcs. Several granites from the Terskey, Kungey, Trans-Ili and Zhetyzhol Ranges were dated with the zircon U/Pb method (SHRIMP, LA-ICP-MS) and yield concordant Late Ordovician–Silurian (~456–420 Ma) emplacement ages. These constrain the "Caledonian" accretion history of the Northern Kyrgyz Tien Shan in the amalgamated Palaeo-Kazakhstan continent. The ancestral Tien Shan orogen assembled in the Early Permian when final closure of the Turkestan Ocean ensued collision of Palaeo-Kazakhstan and Tarim. A Late Palaeozoic structural basement fabric formed and Middle–Late Permian post-collisional magmatism added to crustal growth of the Tien Shan. Permo-Triassic cooling (~300–220 Ma) of the ancestral Tien Shan was unraveled using $^{40}Ar/^{39}Ar$ K-feldspar and titanite fission-track (FT) thermochronology on the Issyk-Kul granitoids. Apatite thermochronology (FT and U–Th–Sm/He) applied to the broader Issyk-Kul region elucidates the Meso-Cenozoic thermo-tectonic evolution and constrains several tectonic reactivation episodes in the Jurassic, Cretaceous and Cenozoic. Exhumation of the studied units occurred during a protracted period of intracontinental orogenesis, linked to far-field effects of Late Jurassic–Cretaceous accretion of peri-Gondwanan blocks from the Tethyan realm to Eurasian. Following a subsequent period of stability and peneplanation, incipient building of the modern Tien Shan orogen in Northern Kyrgyzstan started in the Oligocene according to our data. Intense basement cooling in distinct reactivated and fault-controlled sections of the Trans-Ili and Terskey Ranges finally pinpoint important Miocene–Pliocene (~22–5 Ma) exhumation of the Issyk-Kul basement. Late Cenozoic formation of the Tien Shan is associated with ongoing indentation of India into Eurasia and is a quintessential driving force for the reactivation of the entire Central Asian Orogenic Belt.

1. Introduction

The Tien Shan currently is a more than 2000 km long mountain belt in Central Asia, running from Xinjiang, China in the east to their western counterparts in Kyrgyzstan, Kazakhstan, Uzbekistan, and Tajikistan. The mountain belt is roughly 200 to 300 km wide in north–south direction. Most of the western ranges of the Tien Shan are situated in the Republic of Kyrgyzstan (Fig. 1). This paper deals with the evolution of the Kyrgyz Tien Shan, with a minor amount of samples taken from the most northern ranges in Kazakhstan (Fig. 2). All samples were collected from "basement" rocks (including the crystalline basement sensu stricto, such as metamorphic basement and granitoids). No detrital minerals are used in this study and hence we use the term "basement" in a flexible manner, often implying "non-detrital".

The current, modern Tien Shan orogen developed in the Late Cenozoic, from the Oligocene–Miocene to the present. It currently forms an active intracontinental mountain belt characterized by both fold-and-trust and strike-slip tectonics (Buslov et al., 2003a), developing in between the Kazakhstan (north) and the Tarim (south) microcontinents (Fig. 1). The Late Cenozoic deformation in the Tien Shan can be linked to far-field effects of the continued indentation of

* Corresponding author at: Department of Mineralogy & Petrology, Ghent University, Krijgslaan 281/S8, WE13, B-9000 Ghent, Belgium. Tel.: +32 9264 4564.
E-mail address: Johan.DeGrave@UGent.be (J. De Grave).

1342-937X/$ – see front matter
doi:10.1016/j.gr.2012.06.014

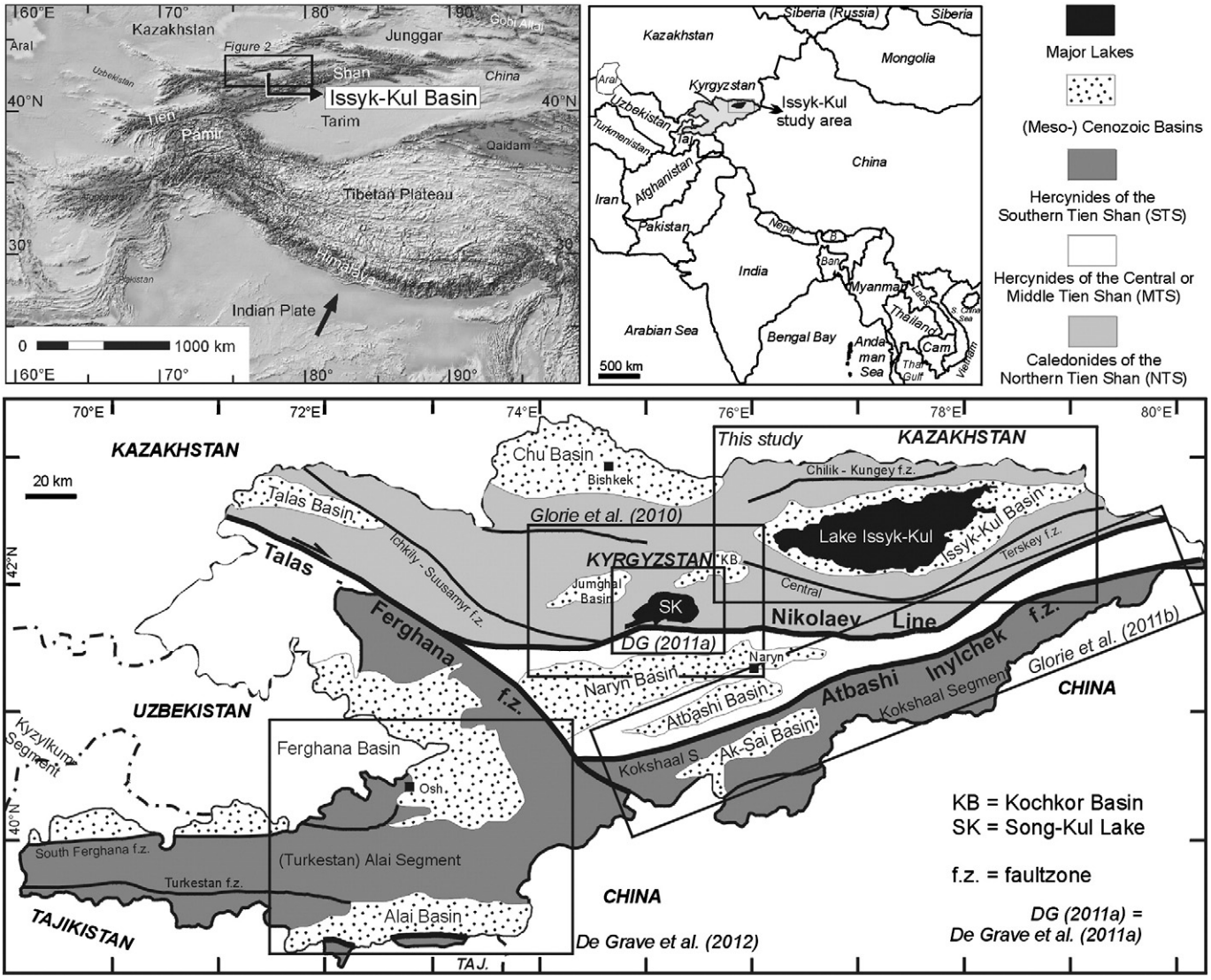

Fig. 1. General location of the Kyrgyz Tien Shan orogen in Central Asia with indication of the Issyk-Kul Basin study area. In Kyrgyzstan the Palaeozoic Tien Shan basement is traditionally subdivided in the Northern, Middle and Southern Tien Shan (NTS, MTS and STS, respectively). The Issyk-Kul Basin and its basement are situated in the NTS; this current study forms part of a broader effort in characterizing the thermo-tectonic history of the Kyrgyz Tien Shan (see outlined boxes).

the Indian continent into Eurasia (Molnar and Tapponnier, 1975). This large-scale collision reactivated the Tien Shan basement structures, eventually building the current intracontinental orogenic edifice. In this broader framework, the Tien Shan forms part of the southern swaths of the vast Central Asian Orogenic Belt (CAOB). More to the north, the CAOB includes other active intracontinental mountain belts such as Gobi-Altai and Altai-Sayan for example. During the Mesozoic, the Tien Shan orogen was subjected to reactivation as distant response to accretion–collision events occurring at the Eurasian margins as well (e.g. Allen and Vincent, 1997; Otto, 1997). These events are cumulatively grouped as the Cimmerian Orogeny, and entail the progressive closure of the Palaeo-Tethyan Ocean and the associated docking of several blocks with Eurasia in a punctuated fashion (Golonka, 2004). Especially the accretion–collision of the Pamir–Tibetan blocks (such as Qiangtang, Lhasa and others) are of crucial importance in relation to the construction of the Mesozoic Tien Shan.

Both the Cenozoic and the Mesozoic tectonics of the Tien Shan mainly transpired through reactivation of more ancient, inherited structures (e.g. Allen and Vincent, 1997; Glorie et al., 2011b). These constitute zones of crustal and lithosperic weakness compared to the more rigid composing basement blocks in the intricate Tien Shan collage. The ancestral Tien Shan basement is predominantly composed of Palaeozoic units that amalgamated throughout the evolution of the so-called Palaeo-Asian Ocean and its sub-basins such as the Terskey and Turkestan Oceans for example (e.g. Windley et al., 2007; Burtman, 2010; Xiao et al., 2010). In this context, the Kyrgyz Tien Shan basement is traditionally subdivided into three units: the Northern (NTS), Middle (MTS) and Southern Tien Shan (STS) (Fig. 1; e.g. Biske and Seltmann, 2010). The NTS contains Precambrian micro-continental units (Kröner et al., 2012), delineated by Cambrian–Ordovician ophiolites, on which Palaeozoic continental magmatic arcs and Meso-Cenozoic basins developed. The NTS is further characterized by large amounts of Early Palaeozoic ("Caledonian"; i.e. Cambrian–Silurian) granitoids which in fact make up a large area of the NTS basement (Fig. 2). Smaller, more isolated Late Palaeozoic ("Hercynian") plutons (Konopelko et al., 2008; Glorie et al., 2010; Seltmann et al., 2011) occur as well. The NTS is separated from the MTS by the Nikolaev Line, a complex Late Palaeozoic sinistral strike-slip fault (Mikolaichuk et al., 1997; Biske and Seltmann, 2010). The MTS basement is mainly composed of Precambrian crust with Neoproterozoic volcanic rocks, covered by Early Palaeozoic sediments and Middle Palaeozoic passive margin sequences. In contrast to the NTS, Early Palaeozoic granitoids are hitherto only described at the southern MTS margin, while Neoproterozoic and Late Palaeozoic plutons are more widely prevalent (e.g. Seltmann et

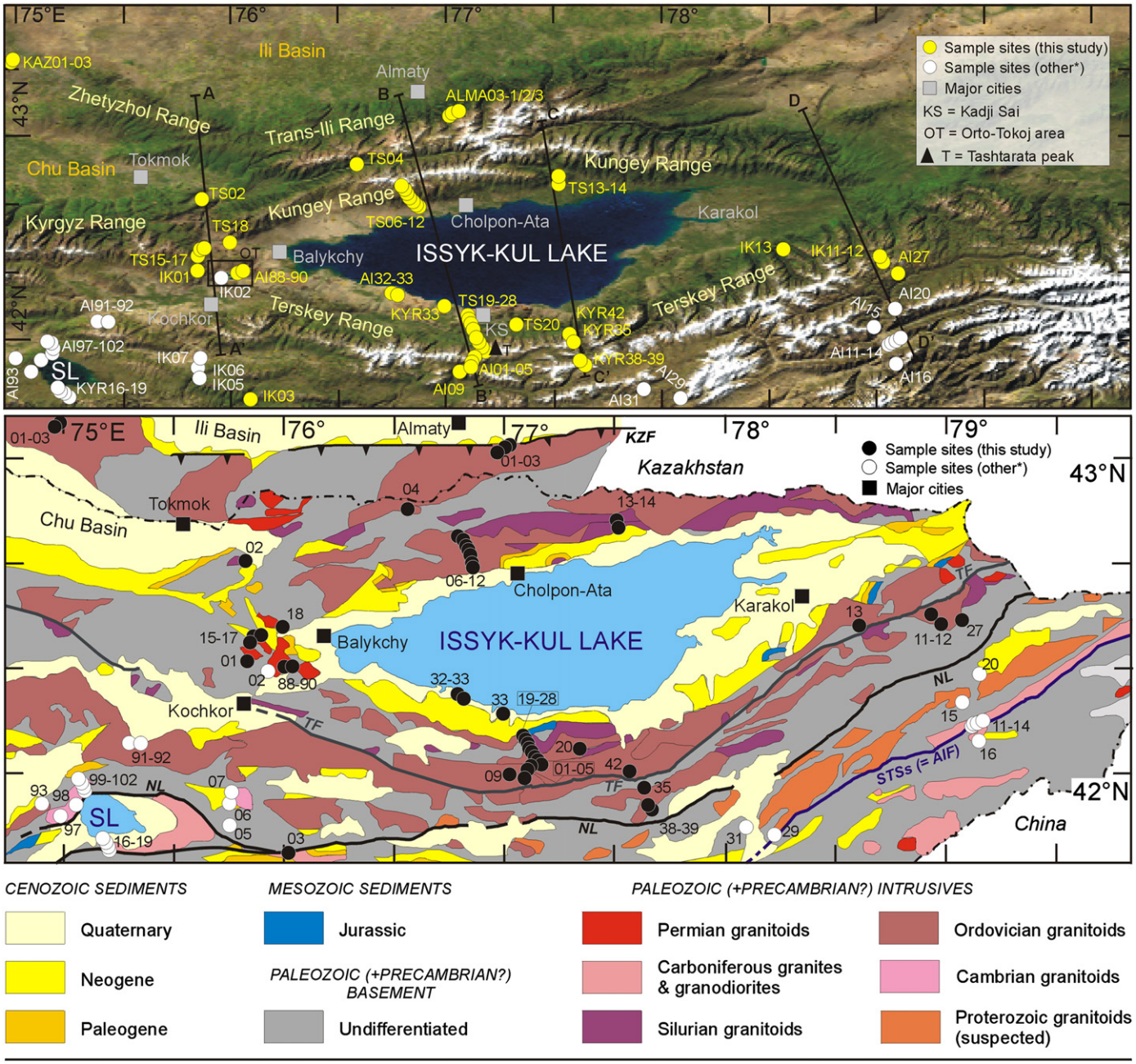

Fig. 2. Top panel: Location of sample sites near the Issyk-Kul Basin. Positions of four profiles (A–A′, B–B′, C–C′ and D–D′, see Fig. 6) are also indicated. Bottom panel: geological sketch map (based on maps by Tursungaziev and Petrov, 2008, and Jenchuraeva et al., 2001) of the basement of the Issyk-Kul area, with the focus on Meso-Cenozoic basins and Palaeozoic intrusive complexes. Sample sites are displayed again. Main faults and structures: KZF = Karakunug–Zaili fault zone, NL = Nikolaev Line, STSs = South Tien Shan suture (also known as AIF = Atbashi–Inylchek Fault), and TF = Terskey Fault. For both panels, sample sites shown as white circles are sites discussed in our previous papers (Glorie et al., 2010; De Grave et al., 2011a; Glorie et al., 2011b). SL = Song-Kul Lake.

al., 2011; Glorie et al., 2011b; Fig. 2). The MTS is separated from the Late Palaeozoic STS collision–accretion complex by the ophiolite-bearing Atbashi–Inylchek or South Tien Shan suture (Alekseev et al., 2007; Biske and Seltmann, 2010; Glorie et al., 2011b).

The Late Palaeozoic granitoids attest to a Permian post-collisional episode of magmatism and are not linked to the more widespread Early Palaeozoic intrusions. They have been dated roughly between 290 and 270 Ma (a comprehensive overview is given by Seltmann et al., 2011). They bear witness to the final building stages of the ancestral Tien Shan in between Palaeo-Kazakhstan and (Kyzylkum-)Tarim. The (post-)collisional deformation associated with these final amalgamation stages led to large-scale strike-slip deformation (e.g. Buslov et al., 2003b), bending of the Kazakhstan orocline (Van der Voo et al., 2006; Abrajevitch et al., 2008; Xiao et al., 2010) and to the inception and reactivation of major shear zones in the ancestral Tien Shan (e.g. Talas–Ferghana fault zone and Karatau ridge; Allen et al., 2001; Alexeiev et al., 2009) and other peripheral palaeo-Kazakhstan units (e.g. Irtysh fault zone; Glorie et al., 2012). These deep-seated structures are often envisaged as important conduits for heat, fluids and partial melts and are therefore closely linked to the occurrence and distribution of post-collisional and/or A-type granitoids (Pirajno, 2010; Glorie et al., 2011b; Seltmann et al., 2011).

The study area on which this paper puts focus is the Issyk-Kul Basin and its underlying basement. This area is entirely located in the NTS unit of the Kyrgyz Tien Shan (Figs. 1, 2). The Issyk-Kul Basin is the most prominent intramontane basin in the modern Kyrgyz Tien Shan orogen. This lenticular shaped basin, elongated in east–west direction (Fig. 2), is

Table 1
Location, lithology and sample details, including the methods used for each sample: AFT = Apatite Fission-Track dating, AHe = Apatite (U–Th–Sm)/He dating, Ar = K-feldspar (microcline or orthoclase) $^{40}Ar/^{39}Ar$ dating, TFT = titanite fission-track dating, ZHe = zircon (U–Th–Sm)/He dating, and ZUPb = zircon U/Pb dating. Results for samples in italic were already (partially) published in Glorie et al. (2010) (*), De Grave et al., 2011a (**), and Glorie et al., 2011b (†).

Sample	Latitude	Longitude	Alt.	Range	Locality	Lithology	Method
TS-02	N42°41′03″	E075°53′21″	1370 m	Kungey Range	Chon Kemin	Granite	AFT
TS-04	N42°51′19″	E076°34′39″	2360 m	Kungey Range	Chon Kemin	Granite	AFT
TS-06	N42°43′35″	E076°49′51″	3950 m	Kungey Range	Orto-Koi-Suu valley	Granite	AFT, AHe
TS-07	N42°43′23″	E076°50′37″	3700 m	Kungey Range	Orto-Koi-Suu valley	Diorite	AFT, TFT
TS-08	N42°43′05″	E076°50′38″	3515 m	Kungey Range	Orto-Koi-Suu valley	Granite	AFT, ZUPb
TS-09	N42°43′01″	E076°50′59″	3300 m	Kungey Range	Orto-Koi-Suu valley	Granite	AFT, TFT
TS-10	N42°43′14″	E076°51′31″	3085 m	Kungey Range	Orto-Koi-Suu valley	Granite	AFT
TS-11	N42°42′17″	E076°51′51″	2860 m	Kungey Range	Orto-Koi-Suu valley	Granite	AFT
TS-12	N42°40′40″	E076°51′03″	2420 m	Kungey Range	Orto-Koi-Suu valley	Granite	AFT, ZUPb
TS-13	N42°46′09″	E077°31′25″	1850 m	Kungey Range	Ak-Suu vall., Kjok Djo.	Granite	AFT, AHe
TS-14	N42°48′07″	E077°31′50″	2080 m	Kungey Range	Ak-Suu vall., Kjok Djo.	Granite	AFT
TS-15	N42°26′57″	E075°51′39″	2150 m	Kyrgyz Range	Tjundjuk valley	Granite	AFT, AHe
TS-16	N42°27′06″	E075°51′23″	1960 m	Kyrgyz Range	Tjundjuk valley	Granite	AFT
TS-17	N42°27′13″	E075°51′25″	1830 m	Kyrgyz Range	Tjundjuk valley	Granite	AFT, AHe
TS-18	N42°27′51″	E076°00′52″	1630 m	Kungey Range	Kara Tash village	Granite	AFT
TS-19	N42°07′11″	E077°08′30″	2020 m	Terskey Range	South of Agat resort	Granite	AFT
TS-20	N42°05′03″	E077°22′04″	2150 m	Terskey Range	Tossor valley	Granite	AFT, TFT
TS-22	N42°03′00″	E077°09′55″	3500 m	Terskey Range	Tashtarata peak	Granite	AFT
TS-23	N42°03′12″	E077°09′31″	3310 m	Terskey Range	Tashtarata peak	Granite	AFT
TS-24	N42°03′16″	E077°09′07″	3080 m	Terskey Range	Tashtarata peak	Granite	AFT
TS-26	N42°04′14″	E077°08′19″	2700 m	Terskey Range	Tashtarata peak	Granite	AFT, AHe
TS-27	N42°05′41″	E077°04′05″	2060 m	Terskey Range	Ak-Terek valley	Granite	AFT
TS-28	N42°07′30″	E077°07′00″	1700 m	Terskey Range	Ak-Terek valley	Granite	AFT
KAZ-01	N43°21′00″	E074°57′00″	1250 m	Zhetyzhol Range	Kur-Dai pass	Granite	AFT, AHe
KAZ-03	N43°14′00″	E074°45′00″	760 m	Zhetyzhol Range	Sjugete village	Qz-diorite	AFT, AHe, ZUPb
IK-01	N42°21′28″	E075°50′49″	2100 m	Kyrgyz Range	Orto-Tokoj lake	Granite	AFT, Ar
IK-03	N41°23′23″	E076°00′41″	2315 m	Naryn Range	Kyzyl-Bel pass	Dolerite	AHe
*IK-02**	*N42°18′35″*	*E075°52′37″*	*1745 m*	*Kyrgyz Range*	*Orto-Tokoj lake*	*Granodiorite*	*AFT, ZUPb*
*IK-05**	*N41°51′34″*	*E075°43′41″*	*2845 m*	*Karadzhorga Range*	*Dolon pass*	*Diabase*	*AFT, AHe*
*IK-06**	*N41°52′50″*	*E075°43′09″*	*2740 m*	*Karadzhorga Range*	*Dolon pass*	*Granite*	*AFT, AHe, ZUPb*
*IK-07**	*N41°55′54″*	*E075°44′14″*	*2450 m*	*Kara-Katta Range*	*Sary Bulak village*	*Granite*	*AFT, Ar*
IK-11	N42°25′22″	E079°01′15″	3200 m	East Terskey Range	Chakir-Korum pass	Sandstone	AFT
IK-12	N42°25′51″	E078°57′04″	2900 m	East Terskey Range	Kjok-Kia base	Granite	AFT, Ar, ZUPb
IK-13	N42°27′07″	E078°33′06″	1970 m	East Terskey Range	Ak-Suu thermal baths	Granite	AFT, AHe, Ar
ALMA3-01	N43°09′48″	E77°02′45″	1640 m	Trans-Ili Range	Malaya Almatinka river	Granite	AFT, TFT, AHe
ALMA3-02	N43°08′55″	E77°03′33″	1960 m	Trans-Ili Range	Malaya Almatinka river	Granite	AFT, TFT, ZUPb
ALMA3-03	N43°07′30″	E77°05′03″	2400 m	Trans-Ili Range	Malaya Almatinka river	Granite	AFT, TFT
*KYR-16***	*N41°45′41″*	*E075°09′38″*	*3090 m*	*Baur-Ala-Bas Range*	*Song Kul Lake*	*Granite*	*AFT, TFT*
*KYR-17***	*N41°43′01″*	*E075°11′19″*	*3720 m*	*Baur-Ala-Bas Range*	*Song Kul Lake*	*Granite*	*AFT*
*KYR-18***	*N41°43′44″*	*E075°11′26″*	*3535 m*	*Baur-Ala-Bas Range*	*Song Kul Lake*	*Granite*	*TFT*
*KYR-19***	*N41°44′16″*	*E075°11′22″*	*3400 m*	*Baur-Ala-Bas Range*	*Song Kul Lake*	*Granite*	*TFT, ZUPb*
KYR-33	N42°05′48″	E077°04′06″	2030 m	Terskey Range	Barskoon village	Granite	AFT
KYR-35	N41°58′11″	E077°38′10″	2450 m	Terskey Range	Barskoon village	Diorite	AFT, ZUPb
KYR-38	N41°52′15″	E077°44′10″	3815 m	Terskey Range	Ara Bel lake	Granite	AFT
KYR-39	N41°54′07″	E077°39′27″	3430 m	Terskey Range	Ara Bel lake	Diorite	AFT, AHe
KYR-42	N42°02′22″	E077°35′52″	2255 m	Terskey Range	Near Barskoon village	Diorite	AFT, TFT
AI-01	N42°02′49″	E077°09′′34″	3435 m	Terskey Range	Tashtarata peak	Granite	AFT
AI-04	N42°02′28″	E077°09′29″	3350 m	Terskey Range	Tashtarata peak	Granite	AFT, ZUPb
AI-05	N42°02′33″	E077°09′09″	3145 m	Terskey Range	Tashtarata peak	Granite	AFT, TFT
AI-09	N42°04′06″	E077°08′40″	2940 m	Terskey Range	Kurumdu valley	Granite	AFT
AI-11†	*N42°02′31″*	*E079°06′10″*	*2470 m*	*Sary Djaz Range*	*Inylchek*	*Granodiorite*	*AFT, TFT, ZUPb*
AI-12†	*N42°03′48″*	*E079°05′19″*	*2950 m*	*Sary Djaz Range*	*Inylchek*	*Granodiorite*	*ZUPb*
AI-13†	*N42°03′51″*	*E079°05′14″*	*2790 m*	*Sary Djaz Range*	*Inylchek*	*Granite*	*AFT, AHe, ZHe, TFT, ZUPb*
AI-14†	*N42°03′45″*	*E079°05′03″*	*2590 m*	*Sary Djaz Range*	*Inylchek*	*Granite*	*AFT, AHe*
AI-15†	*N42°06′40″*	*E079°04′07″*	*2615 m*	*Keoliu Range*	*Inylchek*	*Granite*	*AFT, ZHe, ZUPb*
AI-16†	*N42°01′11″*	*E079°08′25″*	*3500 m*	*Sary Djaz Range*	*Inylchek*	*Granodiorite*	*AFT, AHe, ZHe, ZUPb*
AI-20†	*N42°11′59″*	*E079°06′58″*	*2730 m*	*Sary Djaz Range*	*Keoliu village*	*Granite*	*AFT, AHe, TFT, ZUPb*
AI-27	N42°22′52″	E079°03′12″	3765 m	Terskey Range	Chonasuu pass	Tonalite	AFT
AI-29†	*N41°42′53″*	*E078°09′49″*	*3770 m*	*Akshairak Range*	*Kara Sai valley*	*Mylonite*	*AFT, AHe, ZUPb*
AI-31†	*N41°44′12″*	*E078°03′59″*	*4025 m*	*Djetim Bel Range*	*Arabel pass*	*Tuffite*	*AFT, AHe, ZUPb*
AI-32	N42°08′53″	E076°47′42″	2010 m	Terskey Range	Kokonadyr	Granite	TFT
AI-33	N42°08′45″	E076°47′27″	2220 m	Terskey Range	Kokonadyr	Granite	AFT
AI-88	N42°19′04″	E076°07′39″	1740 m	Terskey Range	Orto-Tokoj lake	Anorthosite	AFT, TFT
AI-90	N42°18′57″	E076°07′42″	1725 m	Terskey Range	Orto-Tokoj lake	Granite	AFT
*AI-91***	*N42°05′35″*	*E075°07′11″*	*2570 m*	*Sandyk Range*	*Kyzart pass*	*Granite*	*AFT, AHe*
*AI-92***	*N42°05′03″*	*E075°04′41″*	*2440 m*	*Sandyk Range*	*Kyzart pass*	*Lamprophyr*	*AFT, ZUPb*
*AI-93***	*N41°53′51″*	*E074°49′25″*	*2290 m*	*Song-Kul Range*	*Sarybulak pass*	*Granite*	*AFT*
*AI-97***	*N41°50′37″*	*E074°54′03″*	*3250 m*	*Song-Kul Range*	*Chilbel pass*	*Diorite*	*AFT, AHe, ZUPb*
*AI-98***	*N41°53′06″*	*E075°01′05″*	*3045 m*	*Song-Kul Range*	*Song-Kul Lake*	*Diorite*	*AFT, ZUPb*
*AI-99***	*N41°55′56″*	*E075°01′44″*	*3515 m*	*Song-Kul Range*	*Song-Kul Lake*	*Diorite*	*AFT, TFT*
*AI-100***	*N41°55′41″*	*E075°02′15″*	*3360 m*	*Song-Kul Range*	*Song-Kul Lake*	*Diorite*	*AFT, AHe, ZUPb*
*AI-101***	*N41°55′08″*	*E075°02′21″*	*3210 m*	*Song-Kul Range*	*Song-Kul Lake*	*Diorite*	*AFT*
*AI-102***	*N41°54′36″*	*E075°02′48″*	*3065 m*	*Song-Kul Range*	*Song-Kul Lake*	*Diorite*	*AFT, AHe*

bordered by the Kungey Range to its north, and the Terskey Range to its south. Both the Kungey and Terskey Ranges extend to the west into the Kyrgyz Range (Fig. 2). North of the Kungey Range, the active sinistral, transpressive Chon Kemin–Chilik Fault (Abdrakhmatov et al., 2002), separates the Kungey Range from the Trans-Ili and Zhetyzhol Ranges in Kazakhstan (Fig. 2). The basement core of the active mountain ranges enclosing the Issyk-Kul Basin is primarily formed by Early Palaeozoic granitoids. The Cenozoic tectonic structure of this study area has been described by many authors (e.g. Abdrakhmatov et al., 2002; Thompson et al., 2002; Bullen et al., 2003; Buslov et al., 2007) and involves both strike-slip deformation (Buslov et al., 2003a) and thrust-and-fold tectonics (Mikolaichuk, 2000).

The Issyk-Kul sediments are purely of continental and/or lacustrine origin and record the tectonic episodes that affected the adjoining basement blocks. The basal units of these sediments are Mesozoic and are only a few hundred meters thick. The basal units consist mainly of Jurassic (quarzitic) sandstones and coal-bearing shales that unconformably overly the Palaeozoic plutonic basement. The Mesozoic sediments are followed by thick Palaeogene, Neogene and Quaternary sequences (Cobbold et al., 1994). The Palaeocene–Eocene Kokturpak Formation (or "Suite" in Russian literature) in the Issyk-Kul Basin is characterized by typical continental red-beds and lacustrine sediments of several hundred meters thick. This Formation is locally intercalated with basaltic and diabasic rocks (Bazhenov and Mikolaichuk, 2002). The Oligocene–Miocene Kyrgyz Formation (up to 2 km thick) of lacustrine sediments shows a general grading upward trend. The Pliocene Issyk-Kul or Chreyskaya Formation (well over 2 km thick) is also composed of lacustrine sediments, with several horizons of coarse clastic sediments (gravels, grits, conglomerates). The Late Pliocene–Early Pleistocene Chapeldak Formation (locally >400 m) consists of gray, coarse, molasse sediments deposited in an alluvial-fan setting. Late Pleistocene and Holocene sediments are characterized by molassic-type deposits, alternated with finer aeolian (loess) and glacial deposits. At present the Issyk-Kul Basin accommodates a deep (up to 668 m) and large (~180 km E–W; ~60 km N–S) intramontane lake: Issyk-Kul Lake (Fig. 2). The lake's sedimentary settings were described in detail by De Batist et al. (2002) and include proximal to distal delta, glacial outwash, mass flow, and current-controlled deposits. The lake bottom has a peculiar morphology with a flat-floored central deep, separated by steep slopes from the surrounding shallower basin floor.

Absolute time constraints on the basement formation, basin development and tectonic evolution of the Issyk-Kul region is limited at best. The driving forces for the several reactivation episodes in the Tien Shan history and the control on these episodes by the inherited structural fabric of the basement is still not fully understood. Therefore, it was opted to implement an integrated multi-method dating strategy to constrain these events of basement formation and amalgamation and subsequent Meso-Cenozoic reactivation of the pre-existent basement structures. The applied methodology is outlined below. The present analysis of the Issyk-Kul region in the NTS forms part of a broader tectono-thermochronometric study (Glorie et al., 2010, 2011b; De Grave et al., 2011a, 2011b), spanning the entire Kyrgyz Tien Shan realm (Fig. 1). For more details on the general geological setting, and the analytical procedures we refer to these papers. Results obtained in these latter studies in general are reflected in the Issyk-Kul Basin area as well. Nevertheless the most extensive sample and data set comes from the Issyk-Kul area and is presented here: 75 new ages are obtained and reported. In tandem with more than 50 published ages from our previous work, around 130 radiometric ages constrain the thermo-tectonic evolution of the NTS basement in an absolute time-frame.

2. Methodology and samples

With the purpose of elucidating the thermo-tectonic evolution of the Issyk-Kul basement from its formation to its present-day outcrop position, several dating techniques were applied: zircon U/Pb dating (ZUPb) (both SHRIMP and LA-ICP-(SF) MS), $^{40}Ar/^{39}Ar$ dating of K-feldspar, titanite fission-track (TFT) dating, apatite fission-track (AFT) and apatite (U–Th–Sm)/He (AHe) thermochronology. Sample details and the methods applied to each individual sample are listed in Table 1. Sample positions are indicated in Fig. 2. As mentioned, in this paper we present 75 new ages (45 AFT, 10 AHe, 10 TFT, 3 $^{40}Ar/^{39}Ar$ and 7 ZUPb) obtained on about 50 samples. Furthermore, published results obtained at our lab from adjoining study areas (60 published ages on about 30 additional samples), were also used to place and interpret the Issyk-Kul data set in the broader Tien Shan context.

ZUPb has a closure temperature in excess of ~800 °C (Cherniak and Watson, 2003) and hence generally records zircon (re)crystallization events when applied to magmatic zircons as done in this paper. Typical magmatic oscillatory zoning (using cathodoluminescence imaging) and magmatic Th/U ratios (between ~0.1 and ~1.0; Hoskin and Schaltegger, 2003; Table 2) were observed for all analyzed samples. The closure temperature for Ar diffusion in K-feldspar is estimated at about 315 °C for orthoclase and is lower, i.e. ~125–185 °C for microcline (McDougall and Harrison, 1999). Debate still exists on the exact closure temperatures of the TFT clock. Most authors cite values in the range of 275–285 °C (e.g. Kohn et al., 1993), while others give a somewhat broader interval of ~265–310 °C (Coyle and Wagner, 1998). The partial annealing zone for fission tracks in apatite depends on apatite crystal chemistry for example, but is largely situated between ~120 and 60 °C (Wagner and Van den haute, 1992; Donelick et al., 2005). For the (U–Th–Sm)/He dating method, He diffusion is blocked around 70–75 °C (Wolf et al., 1996; Ehlers and Farley, 2003) for apatite and ~170–190 °C (Reiners et al., 2004) for zircon. Recent studies on the KTB borehole (Germany) estimated a broader ZHe closure temperature range of ~200–130 °C (Wolfe and Stockli, 2010).

SHRIMP (Sensitive High Resolution Ion Microprobe) ZUPb measurements were carried out at the joint Stanford University — USGS facility with identical set-up and analytical details, including calibration, standards used and data reduction procedures as described in De Grave et al. (2009). Four zircon separates from the Issyk-Kul granitoid basement were dated using this technique (Table 1, Figs. 2, 3): granite sample IK-12 from the eastern Terskey Range, granite samples TS-08 and TS-12 from the central and eastern sections of the Kungey Range respectively, and granite sample ALMA3-02 from the Trans-Ili (or Zaili) Range (close to the Kazakh city of Almaty).

LA-ICP-(SF)-MS (Laser Ablation-Inductively Coupled Plasma-Sector Field-Mass Spectrometry) ZUPb dating was performed at the ICP-MS facility of the Atomic and Mass Spectrometry unit (Dept. Analytical Chemistry, Ghent University), using exactly the same sample preparation and analytical protocols as described in Glorie et al. (2011a). Using this approach, three additional zircon samples were analyzed (Table 1, Figs. 2, 3): samples AI-04 and KYR-35 from the central Terskey Range granites, and diorite sample KAZ-03 from the Zhetyzhol Range in Kazakhstan.

K-feldspar $^{40}Ar/^{39}Ar$ dating results were obtained at the Stanford University Noble Gas Laboratory. Methodological details are as reported in De Grave et al. (2006) and Glorie et al. (2010). K-feldspar composition (i.e. microcline versus orthoclase) was monitored by XRD analysis in order to have a first order estimate of closure temperatures. In this paper we report three new K-feldspar $^{40}Ar/^{39}Ar$ ages (Table 1, Figs. 2, 4) obtained on Terskey Range granitoids. Granite samples IK-12 and IK-13 come from the eastern Terskey Range (Early Palaeozoic granite) and IK-01 from a Late Palaeozoic alkaline granite from the westernmost extremity of the Terskey Range, near Orto-Tokoj (Glorie et al., 2010; Fig. 2). Results from a similar microcline sample (IK-07) from a previous study (Glorie et al., 2010) are also reproduced (Fig. 4). This sample was taken from a granite on the southern fringes of the Terskey Range.

Along with the K-feldspar $^{40}Ar/^{39}Ar$ method, TFT dating is used in this multi-method approach as a 'medium-temperature' range technique, linking the ZUPb data with the low-temperature AFT and

Table 2
Zircon U/Pb dating results for the Issyk-Kul granitoids (average values).

	No.	^{207}Pb[a] (cps)	U[b] (ppm)	Pb[b] (ppm)	Th[b]/U	$^{206}Pb/^{204}Pb$	$^{206}Pb^{c}/^{238}U$	±2σ (%)	$^{207}Pb^{c}/^{235}U$	±2σ (%)	$^{207}Pb^{c}/^{206}Pb$	±2σ (%)	Rho[d]	$^{206}Pb/^{238}U$[e]	±2σ (Ma)	$^{207}Pb/^{235}U$[e]	±2σ (Ma)	Con.[f]
Al 04	1	4330	680	50	0.34	2913	0.0717	3.8	0.5610	5.8	0.0568	4.4	0.66	446	17	452	21	101
	2	3256	513	37	0.32	11839	0.0711	3.5	0.5725	6.1	0.0584	5.0	0.58	443	15	460	23	104
	3	4347	675	49	0.33	15696	0.0723	4.1	0.5763	6.9	0.0579	5.5	0.60	450	18	462	26	103
	4	3188	480	38	0.42	3040	0.0748	3.1	0.6058	6.4	0.0587	5.6	0.48	465	14	481	25	103
	5	707	111	9	0.43	408	0.0727	3.4	0.5704	12.3	0.0569	11.8	0.28	452	15	458	47	101
	6	655	103	8	0.50	249	0.0719	3.3	0.5713	9.6	0.0576	9.0	0.35	448	14	459	36	102
	7	4713	696	55	0.37	1540	0.0763	4.5	0.5988	6.2	0.0569	4.3	0.72	474	20	476	24	101
	8	2545	378	28	0.30	415	0.0742	5.1	0.6202	7.9	0.0606	6.0	0.65	461	23	490	31	106
	9	2097	299	23	0.32	2879	0.0771	3.9	0.6167	7.5	0.0580	6.4	0.52	479	18	488	30	102
	10	1761	269	21	0.52	30478	0.0722	4.1	0.6044	8.0	0.0607	6.8	0.51	450	18	480	31	107
KYR 35	1	2462	383	28	0.33	3419	0.0729	5.1	0.5870	7.9	0.0584	6.1	0.65	453	22	469	30	103
	2	2498	403	29	0.32	1259	0.0714	5.0	0.5657	8.2	0.0575	6.5	0.61	444	22	455	31	102
	3	2231	342	27	0.36	1046	0.0740	4.2	0.5849	8.4	0.0574	7.2	0.50	460	19	468	32	102
	4	1269	201	15	0.48	1342	0.0717	4.5	0.5684	9.7	0.0575	8.6	0.46	447	19	457	36	102
	5	2869	462	36	0.44	1513	0.0742	4.2	0.5570	9.2	0.0545	8.2	0.46	461	19	450	34	97
	6	2387	350	29	0.60	2611	0.0751	4.1	0.6233	7.5	0.0602	6.3	0.55	467	19	492	30	105
	7	5841	938	70	0.26	27083	0.0743	3.5	0.5743	4.9	0.0561	3.4	0.71	462	16	461	18	100
	8	3015	479	35	0.29	10851	0.0721	3.8	0.5701	6.6	0.0573	5.4	0.58	449	16	458	25	102
	9	1261	209	15	0.31	1981	0.0722	2.4	0.5485	6.4	0.0551	6.0	0.38	449	11	444	23	99
	10	1588	268	20	0.44	663	0.0724	4.2	0.5296	8.9	0.0531	7.8	0.48	450	18	432	32	96
	11	2294	372	28	0.38	1256	0.0727	4.5	0.5787	7.9	0.0577	6.4	0.58	452	20	464	30	102
	12	1657	270	20	0.32	1825	0.0741	2.6	0.5664	6.1	0.0555	5.6	0.42	461	12	456	23	99
	13	2868	472	35	0.31	2426	0.0720	3.9	0.5738	6.0	0.0578	4.5	0.65	448	17	460	22	103
	14	3181	544	41	0.45	1239	0.0712	3.0	0.5438	5.4	0.0554	4.5	0.55	443	13	441	20	99
	15	3535	597	44	0.29	2033	0.0738	4.1	0.5534	6.9	0.0544	5.6	0.59	459	18	447	25	97
	16	1431	225	17	0.36	4987	0.0727	3.4	0.5890	7.7	0.0588	6.9	0.44	452	15	470	30	104
	17	3352	555	40	0.28	4318	0.0713	2.9	0.5624	5.7	0.0573	4.9	0.51	444	12	453	21	102
	18	1151	194	14	0.46	971	0.0698	4.1	0.5585	8.4	0.0580	7.4	0.48	435	17	451	31	104
KAZ 03	1	1711	118	9	0.32	591	0.0705	6.2	0.5783	17.7	0.0595	16.6	0.35	439	26	463	68	106
	2	1012	76	6	0.38	246	0.0697	3.0	0.5280	16.3	0.0549	16.0	0.19	435	13	430	59	99
	3	1666	120	9	0.40	305	0.0709	3.8	0.6341	11.0	0.0649	10.4	0.34	441	16	499	44	113
	4	1638	116	9	0.42	416	0.0711	4.1	0.6254	12.4	0.0638	11.8	0.33	443	17	493	50	111
	5	1032	82	6	0.41	544	0.0693	3.3	0.5559	12.7	0.0582	12.2	0.26	432	14	449	47	104
	6	1180	97	7	0.40	274	0.0689	3.8	0.5736	16.9	0.0604	16.5	0.22	429	16	460	65	107
	7	1957	157	12	0.58	10917	0.0714	3.6	0.5824	8.4	0.0592	7.5	0.43	445	16	466	32	105
	8	1473	122	10	0.39	547	0.0739	3.6	0.5844	10.2	0.0574	9.6	0.35	459	16	467	39	102
	9	1237	94	8	0.44	450	0.0726	2.6	0.6389	12.6	0.0638	12.4	0.21	452	12	502	51	111
	10	1875	154	12	0.52	256	0.0705	4.0	0.5952	8.2	0.0613	7.1	0.48	439	17	474	31	108

(continued on next page)

Table 2 (*continued*).

TS 12	1	1388	415	25	0.58	12756	0.0710	1.9	0.5217	2.7	0.0533	1.8	0.72	442	9	426	9	97
	2	2826	854	54	1.04	51051	0.0736	1.9	0.5537	2.2	0.0545	1.2	0.85	456	10	447	8	98
	3	2725	850	51	0.82	4943	0.0701	1.9	0.5289	2.6	0.0547	1.8	0.72	434	9	431	9	99
	4	1113	318	20	0.70	23029	0.0729	1.9	0.5562	2.5	0.0553	1.6	0.78	452	10	449	9	99
	5	447	126	8	0.44	4950	0.0719	2.1	0.5278	4.4	0.0533	3.8	0.48	447	10	430	16	96
	6	3525	1019	62	1.14	5169	0.0703	1.9	0.5317	2.5	0.0548	1.7	0.74	435	10	433	9	100
	7	2971	900	56	0.55	30520	0.0724	1.9	0.5537	2.2	0.0555	1.1	0.87	450	9	447	8	99
	8	2180	614	37	0.97	30914	0.0708	1.9	0.5646	2.3	0.0578	1.3	0.83	438	10	455	8	104
	9	1345	401	25	0.56	7273	0.0735	1.9	0.5728	2.9	0.0565	2.2	0.66	456	9	460	11	101
	10	1898	581	36	0.76	34135	0.0711	1.9	0.5368	2.4	0.0547	1.5	0.78	442	9	436	9	99
IK 12	1	2217	675	40	0.32	16410	0.0689	2.6	0.5200	2.9	0.0547	1.3	0.90	430	12	425	10	99
	2	4301	1259	77	0.36	3990	0.0706	2.6	0.5500	3.2	0.0574	1.8	0.83	439	12	445	12	101
	3	2296	724	43	0.45	22105	0.0697	2.6	0.5307	2.9	0.0552	1.1	0.92	434	12	432	10	100
	4	2336	717	43	0.34	16227	0.0696	2.6	0.5241	3.2	0.0546	1.9	0.81	434	12	428	11	98
	5	3656	1136	68	0.38	62265	0.0698	2.6	0.5418	2.8	0.0563	1.0	0.94	435	12	440	10	101
	6	14127	4504	271	0.39	11115	0.0699	2.6	0.5348	2.7	0.0555	0.7	0.97	435	12	435	10	100
TS 08	1	3200	998	59	0.67	9047	0.0689	2.6	0.5243	3.0	0.0552	1.3	0.89	429	12	428	10	100
	2	1244	366	22	0.76	29733	0.0716	2.7	0.5482	3.0	0.0555	1.5	0.87	446	13	444	11	100
	3	656	196	11	0.99	9061	0.0670	2.7	0.5042	4.5	0.0546	3.6	0.60	418	13	415	16	99
	4	1020	307	19	1.12	99652	0.0704	2.7	0.5367	3.1	0.0553	1.7	0.85	439	14	436	11	99
	5	551	163	10	1.03	3053	0.0678	2.7	0.4992	6.2	0.0534	5.5	0.44	423	13	411	21	97
	6	976	282	17	1.08	6470	0.0702	2.7	0.5277	3.4	0.0545	2.1	0.79	438	14	430	12	98
	7	2483	427	26	0.76	354.1	0.0679	2.7	0.4786	13.6	0.0511	13.4	0.20	423	13	397	46	94
	8	1548	459	28	0.97	89524	0.0701	2.7	0.5419	3.0	0.0560	1.3	0.89	437	13	440	11	101
ALMA 03 02	1	2263	681	40	0.69	15020	0.0680	2.6	0.5151	3.0	0.0549	1.5	0.87	424	12	422	11	99
	2	1139	365	21	0.55	40472	0.0671	2.7	0.5023	3.1	0.0543	1.6	0.86	419	12	413	11	99
	3	1791	554	33	0.53	10401	0.0683	2.6	0.5167	3.3	0.0549	2.0	0.79	426	12	423	12	99
	4	1651	440	26	0.57	1770	0.0672	2.7	0.4981	4.9	0.0538	4.2	0.54	419	12	410	17	98
	5	2554	800	46	0.28	12370	0.0668	2.6	0.5080	3.2	0.0551	1.7	0.84	417	11	417	11	100
	6	3296	1103	63	0.51	32768	0.0667	2.6	0.5019	2.8	0.0546	1.0	0.94	416	11	413	10	99
	7	906	318	18	0.50	5366	0.0667	2.7	0.4896	3.9	0.0532	2.9	0.68	416	12	405	13	97
	8	1396	413	25	1.10	29709	0.0708	2.7	0.5429	3.0	0.0557	1.4	0.88	441	14	440	11	100

[a] Within-run, background-corrected mean ^{207}Pb signal.
[b] U and Pb content and Th/U ratio were calculated relative to the GJ-1 zircon standard.
[c] Ratios corrected for: background, within-run Pb/U fractionation ($^{206}Pb/^{238}U$), common Pb (where necessary) and subsequently normalized to GJ-1 (Instrumental drift corrected).
[d] Rho is the error correlation defined as $err^{206}Pb/^{238}U/err^{207}Pb/^{235}U$.
[e] U/Pb ages were calculated with Isoplot (Ludwig, 2003).
[f] Degree of concordance = $age^{206}Pb/^{238}U/age^{207}Pb/^{206}Pb \times 100$.

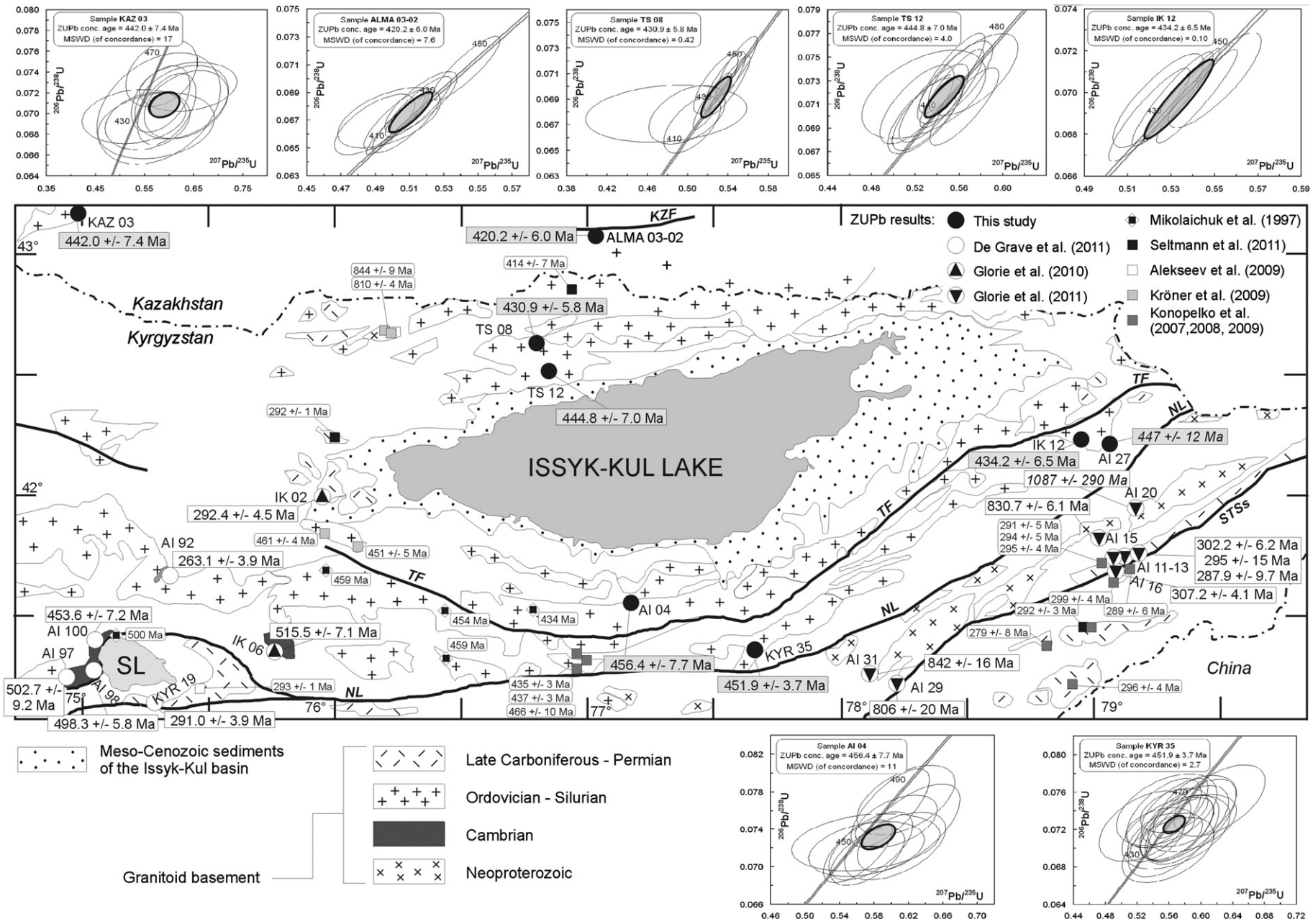

Fig. 3. Schematic geological and tectonic map of the Issyk-Kul basement with indication of the sample sites in the Palaeozoic intrusive complexes where zircon was collected for U/Pb dating (ZUPb). ZUPb results from this study are shown: Concordia plots are given (error ellipses are 2σ, all ages are concordant: shaded ellipse) and ZUPb crystallization ages of the intrusions are indicated on the map (shaded boxes). Similar crystallization ages from our previous studies (Glorie et al., 2010; De Grave et al., 2011a; Glorie et al., 2011b) are indicated (white boxes) along with results from other studies (smaller boxes; Alekseev et al., 2009; Konopelko et al., 2007, 2008, 2009; Kröner et al., 2009; Mikolaichuk et al., 1997; Seltmann et al., 2011). Main faults and structures abbreviated as in Fig. 2. See text for discussion.

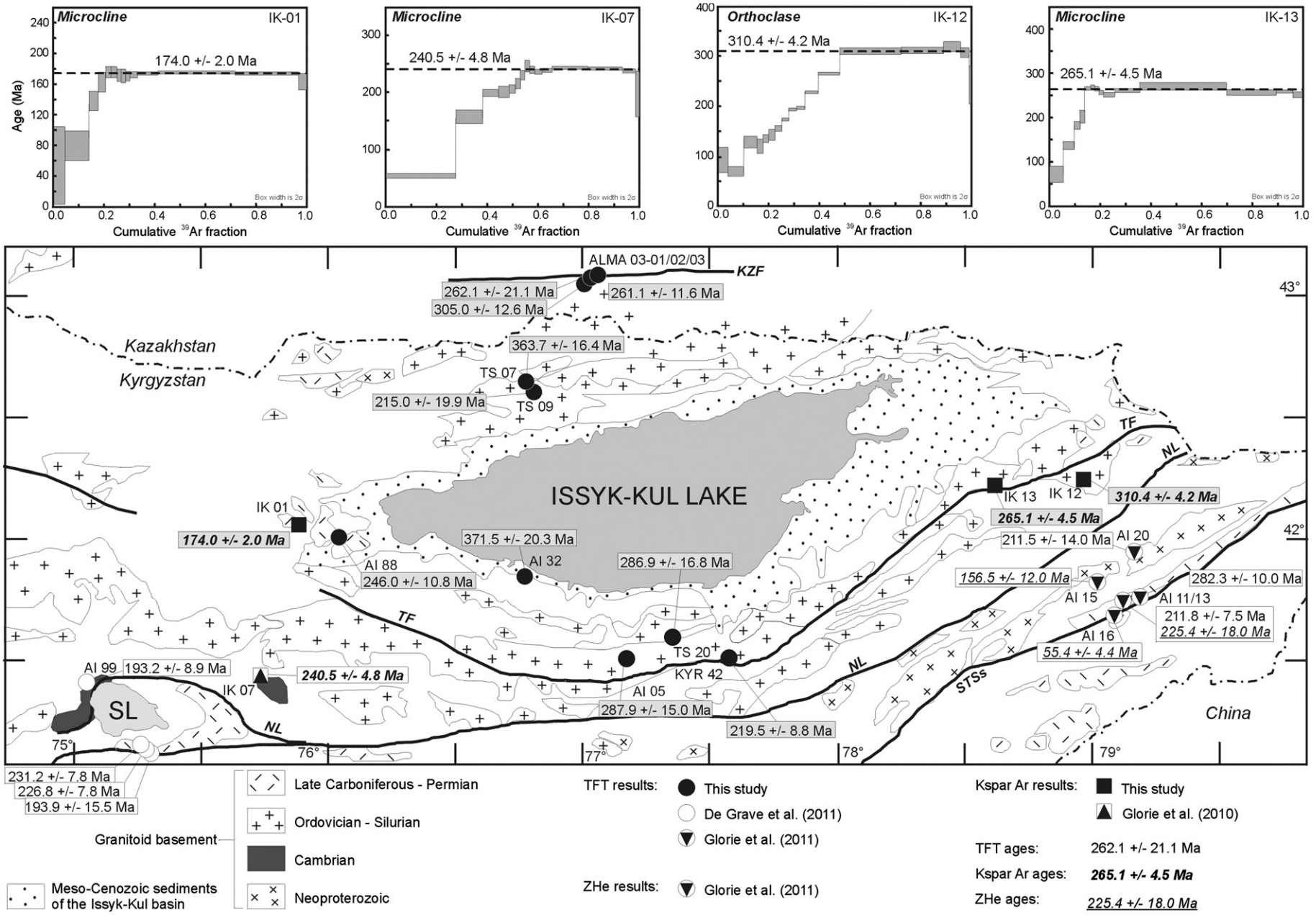

Fig. 4. Schematic geological and tectonic map of the Issyk-Kul basement with indication of the sample sites in the Palaeozoic intrusive complexes for which K-feldspar $^{40}Ar/^{39}Ar$ dating (Kspar Ar), titanite fission-track (TFT) and/or zircon (U–Th–Sm)/He thermochronometry (ZHe) was performed. These three methods are sensitive in the medium temperature range, linking ZUPb and low-T thermochronometry methods (see text for discussion). Results from this study are shown (shaded boxes; Kspar Ar results also as age spectra from stepwise heating experiments). Results from our previous studies (Glorie et al., 2010; De Grave et al., 2011a; Glorie et al., 2011b) are indicated (white boxes) as well. Main faults and structures abbreviated as in Fig. 2. See text for discussion.

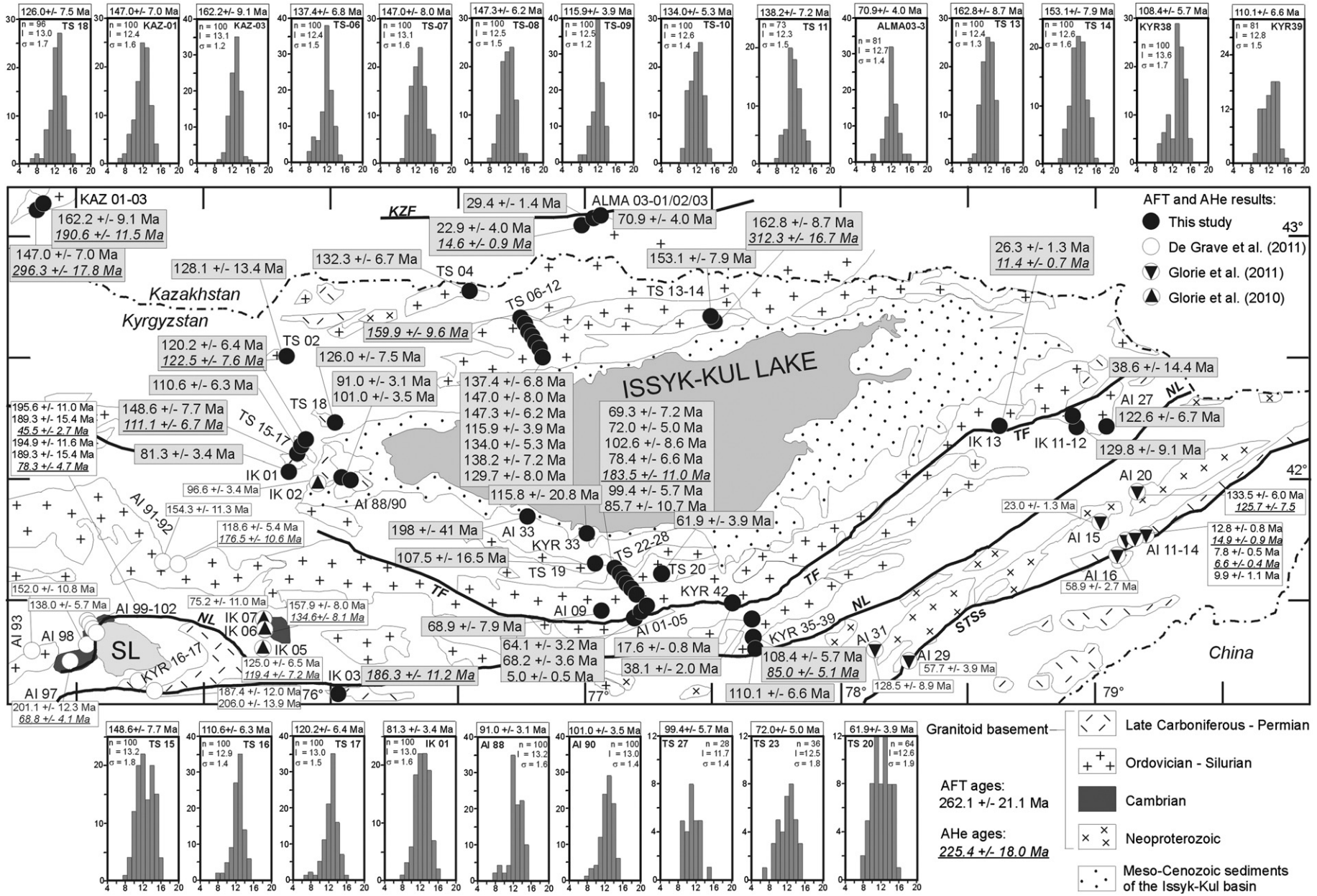

Fig. 5. Schematic geological and tectonic map of the Issyk-Kul basement with indication of the position of the samples to which low-T thermochronometry methods were applied: apatite fission-track (AFT) and/or apatite (U–Th–Sm)/He thermochronometry (AHe). Results from this study are shown (shaded boxes; results for AFT length measurements are displayed as length–frequency-distribution histograms). Results from our previous studies (Glorie et al., 2010; De Grave et al., 2011a; Glorie et al., 2011b) are indicated (white boxes) as well. Main faults and structures abbreviated as in Fig. 2. See text for discussion.

AHe thermochronometric methods discussed below. Analytical details, including zeta calibration, thermal neutron irradiation and monitoring, and etching protocols for the TFT analyses performed in this study are identical with those published by De Grave et al. (2011a) and De Grave et al. (2011c). Ten new TFT ages are presented here (Table 1, Figs. 2, 4). Three TFT ages were obtained from the Trans-Ili granites close to Almaty (samples ALMA03-01, 02 and 03), two were obtained from the granitoid basement of the Kungey Range (TS-07 and TS-09), four from the central Terskey Range (AI-05, AI-32, TS-20, and KYR-42), and finally one titanite separate from sample AI-88 (Orto-Tokoj alkaline intrusion) in the western Terskey Range.

AFT thermochronometry was applied to 45 samples from all adjoining basement blocks (almost exclusively granitoids) to the Issyk-Kul Basin (Table 1, Figs. 2, 5). This data also includes several vertical profiles, most notably in the central Kungey Range (up Orto-Koi-Suu valley, north of Cholpon-Ata, Fig. 2) and in the central Terskey Range (Tashtarata massif, south of Bokonbaeva and Kadji Sai villages) (Fig. 2). Specifics on AFT sample preparation, calibration (zeta and absolute thermal neutron monitoring), etching conditions, track observation, length measurements, and numerical modeling strategy (performed with HeFTy, Ketcham, 2005) are to be found in several recent papers (e.g. De Grave et al., 2009, 2011a, b, c; Glorie et al., 2010; 2011b; 2012).

AHe measurements were carried out at the thermochronology laboratory of Kansas State University and analytical conditions and settings are the same as outlined in previous papers (e.g. De Grave et al., 2009, 2011a, b, c; Glorie et al., 2010, 2011b, and references therein). We present 11 new AHe ages for samples in the Issyk-Kul basement (Table 1, Figs. 2, 5). Additional ZHe results were reproduced from samples in the South Tien Shan basement and are by Glorie et al. (2011b). These ZHe ages constrain the timing of incipient, ongoing tectonic activity and are also used (in tandem with TFT and K-feldspar $^{40}Ar/^{39}Ar$ ages) as a higher temperature benchmark for AFT and AHe thermochronometry.

3. Results and discussion

3.1. Zircon U/Pb ages and Palaeozoic assembly

Our ZUPb results indicate that the granitoid basement of the Issyk-Kul Basin formed in the Early Palaeozoic. Specifically, Late Ordovician–Silurian ("Caledonian") zircon crystallization ages (Table 2, Fig. 3) between 456 and 420 Ma were found. The younger ages were obtained in the northern part of the Issyk-Kul basement. Zircons from granite sample ALMA3-02 in the Trans-Ili Range and from quartz diorite KAZ-03 in the Zhetyzhol Range yield Late Silurian ages of 420 ± 5 Ma (SHRIMP) and 422 ± 6 Ma (LA-ICP-MS), respectively (Table 2, Fig. 3). These results correspond with a ZUPb age of 414 ± 7 Ma published recently (Seltmann et al., 2011) for the Aktyuz granitoids in between the Trans-Ili and Kungey Ranges (Fig. 3). The Kungey Range forms the northern boundary of the present-day Issyk-Kul Basin and granites sampled here (TS-08 and TS-12) have Early Silurian crystallization ages of 431 ± 6 Ma and 445 ± 7 Ma (Table 2, Fig. 3; SHRIMP). These ages are similar to those obtained for the southern Issyk-Kul margin (Terskey Range granitoids): 434 ± 7 Ma (eastern Terskey granite, IK-12, SHRIMP) and 452 ± 4 Ma to 456 ± 8 Ma (central Terskey, KYR-35 diorite and AI-04 granite, LA-ICP-MS; Table 2, Fig. 3) which extend into the Late Ordovician. Several authors report similar Late Ordovician–Early Silurian ages between about 460–435 Ma from the Terskey Range (Mikolaichuk et al., 1997; Konopelko et al., 2008; Kröner et al., 2009; Fig. 3) and for other areas in the NTS Mikolaichuk et al., 1997; Konopelko et al., 2008). Also in the Chinese Tien Shan these observation are made (e.g. Gao et al., 2009; Yang and Zhou, 2009; Dong et al., 2011; Wang et al., 2012).

In our study area, the somewhat younger ZUPb ages of ~420 Ma (latest Silurian) only occur in the current northernmost granitic basement of the Kyrgyz–Kazakh Tien Shan. Similar results by Seltmann et al. (2011) seem to extend this time frame to the earliest Devonian. It is still not clear if this latest Silurian–earliest Devonian episode of granitic intrusion really represents a distinct magmatic episode or if it is a regional expression of diachronous closure of the ancient Tien Shan oceanic basins. When considering it as a distinct event, it is not evident at this moment in what geodynamic context this magmatism should be viewed. Seltmann et al. (2011) suggest a back-arc extensional setting based on the palaeogeographic position of the sample sites.

The Ordovician–Silurian subduction related granitoids make up a large part of the crystalline basement of Issyk-Kul Basin and occur in fact widespread in the entire NTS. They are thought to form part of an extensive Andean-type continental arc that was constructed on the accretionary orogenic rim of palaeo-Kazakhstan and extends further north (present-day co-ordinates) into this amalgamated microcontinent, possibly linking up with the Kokchetav terrane (Northern Kazakhstan) (e.g. Windley et al., 2007; Xiao et al., 2010; Kröner et al., 2012) where similar ages are found (e.g. Zhimulev et al., 2011). These granitoids were emplaced due to closure and subduction of the so-called Palaeo-Asian Ocean (PAO) (Khain et al., 2003). The Terskey and Turkestan Oceans that played a pivotal role in the (Kyrgyz) Tien Shan basement

Table 3
TFT age data: n is the number of counted grains; ρ_s, ρ_i, and ρ_d are the density of spontaneous, induced tracks and induced tracks in an external detector (ED) irradiated against a dosimeter glass. The ρ_d-values are interpolated values from regularly spaced glass dosimeters (IRMM-540). ρ_d is expressed as 10^5 tracks/cm^2; ρ_s and ρ_i are expressed as 10^6 tracks/cm^2. N_s, N_i, and N_d are the number of counted spontaneous, induced tracks and induced tracks in the ED. N_d is an interpolated value. P (χ^2) is the chi-squared probability that the dated grains have a constant ρ_s/ρ_i-ratio. An ζ-value of 505.1 ± 7.8 a·cm^2 was used for the calculation of the TFT age t_ζ (in Ma). Absolute ages (Q-ages), t_Q, are listed as well to illustrate the compatibility of both calibration systems and to underscore the 'stable' observation efficiency of the tracks in titanite (OWMQ = 1.910 ± 0.070 based on Fish Canyon Tuff and Mount Dromedary titanite; De Grave et al., 2011a).

Sample	n	ρ_s (±1σ)	N_s	ρ_i (±1σ)	N_i	ρ_d (±1σ)	N_d	ρ_s/ρ_i	P (χ^2)	t_ζ	t_Q
Trans-Ili Range											
ALMA03-1	18	12.790 (0.208)	3778	4.224 (0.120)	1243	4.036 (0.079)	2583	3.064 ± 0.100	0.45	305.0 ± 12.6	303.5 ± 16.7
ALMA03-2	6	10.411 (0.426)	597	4.356 (0.282)	238	4.019 (0.079)	2572	2.635 ± 0.202	0.58	262.1 ± 21.1	261.8 ± 23.2
ALMA03-3	15	11.052 (0.215)	2653	4.346 (0.135)	1043	4.001 (0.079)	2561	2.637 ± 0.096	0.21	261.1 ± 11.6	262.0 ± 15.1
Kungey Range											
TS-07	15	13.779 (0.240)	3306	3.758 (0.125)	902	3.993 (0.079)	2555	3.710 ± 0.139	0.79	363.7 ± 16.4	365.7 ± 21.3
TS-09	5	8.129 (0.406)	401	3.765 (0.278)	183	3.994 (0.079)	2556	2.167 ± 0.193	0.82	215.0 ± 19.9	216.1 ± 21.5
Kyrgyz–Kungey Range transition (Kyzylkompol Ridge)											
AI-88	16	10.932 (0.214)	2607	4.633 (0.139)	1114	4.007 (0.079)	2564	2.478 ± 0.089	0.36	246.0 ± 10.8	246.5 ± 14.1
Terskey Range											
TS-20	9	12.101 (0.321)	1463	4.282 (0.196)	479	3.997 (0.079)	2558	2.906 ± 0.154	0.63	286.9 ± 16.8	288.2 ± 19.8
AI-05	11	15.088 (0.352)	1837	5.316 (0.209)	647	4.011 (0.078)	2622	2.907 ± 0.096	0.69	287.9 ± 15.0	288.3 ± 18.4
AI-32	10	17.160 (0.381)	2032	4.526 (0.196)	534	3.970 (0.079)	2541	3.814 ± 0.185	0.96	371.5 ± 20.3	375.6 ± 24.7
KYR-42	17	13.212 (0.232)	3254	6.133 (0.158)	1514	3.986 (0.079)	2551	2.218 ± 0.069	0.08	219.5 ± 8.8	221.1 ± 12.0

development (e.g. Burtman, 2010), are considered as sub-basins of the PAO (Windley et al., 2007). The main phase of this "Caledonian" episode of accretionary and collisional tectonics is 460–430 Ma (possibly prolonged to ~420 Ma, see previous paragraph). Our results thus confirm these findings and expand the data-set into the hitherto undated granitoids of the Issyk-Kul basement. At the cessation of the Early Palaeozoic events, the Palaeo-Kazakhstan microcontinent was assembled and the NTS and MTS units of the Tien Shan were incorporated in its orogenic rim. The Turkestan or Southern Tien Shan Ocean still separated Palaeo-Kazakhstan from (Kyzylkum-)Tarim. Convergence of these two major CAOB blocks led to the closure of the Turkestan Ocean and their eventual collision (Burtman, 2010; Xiao et al., 2010). Late Palaeozoic post-collisional granitoids that cross-cut tectonic boundaries in the Tien Shan edifice, illustrate the final stitching of the ancestral Tien Shan composing units.

Minor amounts of these Late Palaeozoic ("Hercynian") post-collisional granitoids occur in the Issyk-Kul basement. They occur in particular in the Orto-Tokoj area where the current three major mountain ranges of the western Issyk-Kul area (Kungey, Terskey and Kyrgyz Range) converge (e.g. sample site IK-02) (Glorie et al., 2010; Seltmann et al., 2011). These granitoids are related to a Permian post-collisional episode of magmatism as explained in the introduction section earlier.

3.2. Titanite fission track (TFT) and K-feldspar $^{40}Ar/^{39}Ar$ ages and the Permo-Triassic Tien Shan

In this paper we present the first TFT ages obtained from the granitic basement of the Issyk-Kul Basin. Titanites from ten sample sites were dated: three from the Trans-Ili Range, two from the Kungey Range, four from Terskey Range and one sample from the Orto-Tokoj area (Table 3, Fig. 4). The TFT Partial Annealing Zone (PAZ) is the temperature (T) range where fission tracks in titanite are considered to be partially stable; i.e. they will accumulate over time, but will be subjected to partial annealing and shortening. The TFT PAZ is defined as a relatively wide interval of ~265–310 °C (Coyle and Wagner, 1998), while other authors define a more narrow range of 275–285 °C (e.g. Kohn et al., 1993). At higher temperature spontaneous tracks are not retained in titanite and in these conditions the TFT system is hence not a closed radiometric dating system. TFT ages can therefore be interpreted as cooling ages. Post-magmatic or post-deformation relaxation of the crustal isotherms are possible mechanisms for such basement cooling. The TFT results obtained from the Issyk-Kul granitoids exhibit a broad Late Palaeozoic–Early Mesozoic age range from 372 to 215 Ma (i.e. Late Devonian to Late Triassic). Most TFT ages however are Permo-Triassic and are situated roughly between 300 and 220 Ma. The TFT ages were calculated based on age standards using zeta (ζ) calibration as well as with absolute methods (absolute thermal neutron fluence monitoring; De Grave et al., 2011a). Table 3 indicates that both calibration methods yield identical ages. In this discussion the more conventional ζ-ages are used.

The Trans-Ili Range granites yield two consistent Late Permian TFT ages of 262 ± 21 Ma and 261 ± 12 Ma and one somewhat older sample of 305 ± 13 Ma (near Carboniferous–Permian transition) (Table 3, Fig. 4). These Permian ages are clearly significantly younger than the Late Silurian (~420 Ma) ZUPb emplacement ages of the granites and hence the TFT ages cannot be interpreted here as post-magmatic cooling ages.

The two TFT ages from the Kungey Range (Table 3, Fig. 4) range between 364 ± 16 Ma (TS-07) and 215 ± 20 Ma (TS-09). Latter Late Triassic age shows good similarities with TFT and AFT ages obtained from the Song-Kul area in the Kyrgyz Tien Shan (De Grave et al., 2011a). This Late Triassic age might be related to a distinct Mesozoic reactivation event (see further). Sample TS-09 was not dated with the ZUPb method, but granite sample TS-07 from the same massif yielded an emplacement age associated with the Late Ordovician–Early Silurian main phase of subduction related magmatism. The Late Devonian–Early Carboniferous TFT age of 364 ± 16 Ma for sample TS-09 can therefore not be related to post-magmatic cooling of the Early Palaeozoic granitoids and hence either dates a distinct Middle Palaeozoic event or represents a TFT PAZ residence age of slowly cooled basement.

More or less the same spread in TFT ages is observed for the Terskey Range samples for which ages of 372 ± 20 Ma (AI-32) and 220 ± 9 Ma (KYR-42) were found. Both of these can readily be understood along the same lines as outlined above for the Kungey samples: a Late Devonian–Early Carboniferous TFT PAZ residence age with no specific geological meaning (AI-32) and a Late Triassic reactivation age (KYR-42). Note that the latter "reactivated" sample comes from within the Terskey fault zone (Fig. 4), while AI-32 was not taken in close vicinity of a major fault. Two other samples of Terskey granites (TS-20 and AI-05) yield consistent Early Permian ages of ~287 Ma and within analytical uncertainty can be considered identical to the TFT ages in the Trans-Ili Range (Table 3, Fig. 4). These latter samples were collected close to the Terskey fault, but not in the fault zone itself as was the case for KYR-42. Similar as for the Kungey Range samples, the Terskey Range TFT ages are disconnected from post-magmatic cooling of the Early Palaeozoic arc. Sample AI-88 is an alkaline anorthosite from a Permian post-collisional pluton near Orto-Tokoj. Its TFT age was established as 246 ± 11 Ma. This Early to Middle Triassic TFT age implies an age gap of about 40–45 Ma with its emplacement age, shown to be 292 Ma (Glorie et al., 2010). Although some minor influences of post-magmatic cooling cannot be ruled out here, the TFT age does seem to point toward a separate Triassic event. This hypothesis is underscored by similar ages (various thermochronometers) in other sample areas around Issyk-Kul Basin (e.g. Song-Kul area; De Grave et al., 2011a).

K-feldspar $^{40}Ar/^{39}Ar$ ages were obtained from 3 locations in the Terskey Range (Fig. 4). The composition of the K-feldspar separates was monitored using XRD analysis. The separates did not represent a pure polymorph, but proved to be a mix between orthoclase and microcline. Orthoclase was distinguished by its pinkish to light orange color, while microcline was white. Pinkish orthoclase from two samples in the eastern Terskey Range, IK-12 and IK-13, were prepared for resistance furnace stepwise heating $^{40}Ar/^{39}Ar$ dating and yielded well-defined plateau ages of 310 ± 4 Ma and 265 ± 5 Ma, respectively. The younger, Middle Permian (IK-13) sample comes from within the Terskey fault zone, while the older (Late Carboniferous) IK-12 was taken some distance away (Fig. 4). Orthoclase Ar-closure temperatures are considered to be similar (or only slightly higher at ~310 °C; McDougall and Harrison, 1999) to that of the TFT system, and hence these ages can be compared directly. Microcline from sample IK-01, from the Permian Orto-Tokoj granitoids yielded a $^{40}Ar/^{39}Ar$ age of 174 ± 2 Ma. Microcline is the lower-T polymorph of orthoclase and its closure temperature for Ar diffusion is significantly lower than for orthoclase (~125–185 °C as compared to ~310 °C; McDougall and Harrison, 1999). It is therefore more complementary to the AFT thermochronometer (~60–120 °C). As shown in the next section, the Middle Jurassic microcline $^{40}Ar/^{39}Ar$ age links up quite well with the AFT ages of the Issyk-Kul basement rocks. In addition, Glorie et al. (2010) reported a Middle Triassic microcline Ar-age for a granite in the Kara-Katta Range, south of the Terskey Range (Fig. 4).

In the latest Carboniferous–Early Permian the ancestral Tien Shan was formed when the last Turkestan Ocean tracts closed and the amalgamated Palaeo-Kazakhstan microcontinent (including NTS and MTS) collided with Tarim and the STS collision–accretion complex in between. Late Carboniferous–Early Permian collisional granites with ZUPb ages ranging between about 315 and 295 Ma attest to this event as outlined in a previous paragraph (e.g. Alekseev et al., 2009; Biske and Seltmann, 2010; De Grave et al., 2011a; Seltmann et al., 2011). Final amalgamation of the ancestral Tien Shan seems to have occurred diachronously and started somewhat earlier in the Chinese Tien Shan areas (e.g. Chen et al., 1999; 2011; Gao et al., 2009; Han et al., 2011; Seltmann et al., 2011). Final amalgamation

of the Tien Shan was quickly followed by distinct post-collisional magmatism, often related to reactivation and formation of shear zones (e.g. Van der Voo et al., 2006; Abrajevitch et al., 2008). Permian post-collisional A-type intrusions are dated to about 295–280 Ma (e.g. Konopelko et al., 2007, 2009; Glorie et al., 2011b; Seltmann et al., 2011). Further minor alkaline magmatism is also observed and is represented for example by lamprophyre dykes and carbonatites. Their ZUPb ages are reported as 275–260 Ma (De Grave et al., 2011a, 2011b). Seltmann et al. (2011) and Glorie et al. (2011b) further argue for a Triassic (~240–215 Ma) thermal event in the Kyrgyz Tien Shan as deduced from Triassic zircon grains and overgrowths in magmatic rocks closely related to Permo-Triassic shear zones. This is additionally underpinned by Triassic $^{40}Ar/^{39}Ar$ ages on mica and K-feldspar from shear zone related rocks (e.g. Wilde et al., 2001).

Results from several thermochronometers sensitive in "medium-temperature" ranges – such as TFT and K-feldspar $^{40}Ar/^{39}Ar$ dating used in this study (De Grave et al., 2011a; Glorie et al., 2010, 2011b) – point toward an important Permo-Triassic cooling event affecting the Issyk-Kul area and adjoining regions. Additional ZHe data further constrain this event in other Tien Shan areas as well (Glorie et al., 2011b). Most of the ages from these different "medium-thermochronometers" fall in the range of 280–210 Ma, i.e. roughly Middle Permian to Late Triassic. Two Late Devonian (~370–360 Ma) ages (Fig. 4) are not considered here as explained above. The Middle Permian–Early Triassic ages from this study are concentrated along major Palaeozoic faults and shear zones in the Issyk-Kul basement such as the Terskey fault, south of Issyk-Kul Basin and the Zaili and Kemin faults in the north (Fig. 4). This also holds true for the other studies mentioned with sample sites in and near the Nikolaev Line (Glorie et al., 2010; De Grave et al., 2011a) and the Atbashi–Inylchek fault (= South Tien Shan suture) (Glorie et al., 2011b). These features are mainly "Hercynian" structures that experienced one or more subsequent reactivation phases. The somewhat deviant Late Carboniferous (~310–305 Ma) ages might be interpreted as "inception" of these fault systems or cooling after heat transport along them. The more widespread Permo-Triassic ages allude to a regional scale tectonic reactivation, possibly related to large scale strike-slip faulting and lateral displacements, that occurred after the Tarim collision and final amalgamation of the ancestral Tien Shan. Chronological evidence for this event comes from resetting in some zircon grains across the entire Tien Shan edifice and zircon overgrowths in fault systems (Glorie et al., 2011b; Seltmann et al., 2011), from Ar-thermochronology (e.g. Wilde et al., 2001) and from TFT thermochronology in for example the Song-Kul area (De Grave et al., 2011a) and the STS (Glorie et al., 2011b). In the Song Kul area, this Triassic event is even preserved in the AFT ages of the crystalline basement (De Grave et al., 2011a).

The "medium-T range" thermochronometric data show that the fault systems that formed during final amalgamation of the ancestral Kyrgyz Tien Shan in the Late Carboniferous–Early Permian almost seamlessly progressed in a Permo-Triassic reactivation episode. This tectonic activity and basement heating and cooling is coeval with the onset of so-called Cimmerian collisions on the southern Eurasian margin on one hand, strike-slip tectonics, extension and subsidence in Tarim and the development of a supposed Large Igneous Province (LIP) in the Tarim Basin on the other. Rocks associated with this Permian (Triassic) Tarim LIP or Bachu LIP (Zhang et al., 2010a) are to a large extent buried by thick Meso-Cenozoic sediments. Exposed alkaline basalts however were dated to ~285–260 Ma (Middle–Late Permian; Zhang et al., 2010b; Qin et al., 2011); associated more differentiated rocks to ~290–270 Ma (Early Permian; Zhang et al., 2008; Tian et al., 2010; Li et al., 2011a, 2011b).

Collisional orogenesis resumed at the southern Eurasian margin during the Middle Triassic with e.g. closure of the Palaeo-Tethys Ocean and the subsequent accretion of several tectonic units (Golonka, 2004). An important example is the Cimmerian Qiangtang block that was added to the Kunlun terrane of the South Eurasian margin during the Middle–Late Triassic (~240–200 Ma). This occurred along the Jinsha suture south of Tarim, in present-day Tibet and the Pamirs (Ratschbacher et al., 2003; Schwab et al., 2004; Pullen et al., 2008; Zhai et al., 2011). A remnant oceanic basin, the Songpan–Ganzi Ocean was finally closed in the Late Triassic (~210 Ma; Pullen et al., 2008; Wang et al., 2011). The Triassic collision of a related Cimmerian unit, the Turan plate to the west of the Pamir block also plays a role in the Early Mesozoic reactivation in the Tien Shan (e.g. Alexeiev et al., 2009).

3.3. Apatite thermochronology and building of the Meso-Cenozoic Kyrgyz Tien Shan

Apatite fission track (AFT) results represent the major part of the data-set provided in this paper. All AFT ages are Meso- and Cenozoic (i.e. Early Jurassic to Pliocene), with the oldest age of 198 ± 41 Ma (AI-33) and the youngest age of 5.0 ± 0.5 Ma (AI-05) (Table 4, Fig. 5). The aforementioned oldest sample may be regarded as an outlier as most other older samples exhibit Middle to Late Jurassic ages. However, due to the rather large uncertainty, this Early Jurassic age also overlaps within error with the Middle to Late Jurassic age cluster and is discussed in this context. Besides this Jurassic age cluster, we distinguish an Early Cretaceous (~150–130 Ma), a Middle Cretaceous (~110–90 Ma) and a Late Cretaceous (~75–65 Ma) age cluster. Finally an Oligocene–Pliocene (~35–5 Ma) AFT age group is found in our study area.

The Jurassic age group contains an isolated sample from the Orto-Tokoj area (TS-15) with an AFT age of 149 ± 8 Ma and a relatively broad AFT length distribution ($\sigma = 1.8$ μm) with a mean of 13.2 μm. The samples from the Zhetyzhol Range in Kazakhstan (KAZ-01 and KAZ-03) are also included here and yield apparent ages of 147 ± 7 and 162 ± 9 Ma and mean track lengths (MTL) of 12.4 μm ($\sigma = 1.6$ μm) and 13.1 μm ($\sigma = 1.2$ μm), respectively (Table 4, Fig. 5). In the eastern section of the Kungey Range, samples TS-13 and TS-14 yield comparable AFT results with respective ages of 163 ± 9 Ma and 153 ± 8 Ma and MTL values of 12.4 μm ($\sigma = 1.3$ μm) and 12.6 μm ($\sigma = 1.6$ μm).

The AFT ages for the central Kungey Range profile along the Orto-Koi-Suu valley (north of Cholpon-Ata village) are somewhat younger and can in general be labeled as Early Cretaceous. This vertical sample profile involves seven samples (TS-06 to TS-12) with ages ranging between 147 ± 8 Ma and 130 ± 8 Ma. Sample TS-09 is an exception and is slightly younger (116 ± 4 Ma). AFT length data is nearly identical for all samples from this profile with MTL values clustering around 12.5 μm ($\sigma = 1.5$ μm) and are hence comparable to the Jurassic samples in that respect. Just north of the Kungey Range, the samples from the Chon Kemin fault zone (TS-02 and TS-04) also have Early Cretaceous AFT ages of 128 ± 13 Ma and 132 ± 7 Ma, respectively (Table 4, Fig. 5). The amount of measurable confined tracks was insufficient for the Chon Kemin samples and consequently no length data can be reported. TS-18 from the westernmost Kungey foothills (126 ± 8 Ma, MTL = 13.0 μm, $\sigma = 1.7$ μm) can be considered here as well. A few isolated samples from the eastern Terskey Range can also be included in this Early Cretaceous age cluster (e.g. AI-27: 123 ± 7 Ma and IK-11: 130 ± 9 Ma).

However, the bulk of the AFT ages for the Terskey Range samples and adjoining areas are Middle to Late Cretaceous. In the Orto-Tokoj and Kyzylkompol Ridge area, at the western end of the Issyk-Kul Basin, samples yield Middle and Late Cretaceous AFT ages (Table 4, Fig. 5). Sample TS-15 has an older, Late Jurassic age as discussed above. Most ages in fact range between ~100 and 90 Ma. Modest outliers are TS-16 at the oldest (111 ± 6 Ma) and IK-01 (81 ± 3 Ma) at the youngest end of the spectrum. Mean track lengths are in general slightly longer as for the previously discussed data and are around 13.0 μm ($\sigma = 1.5$ μm). Samples from the highest Terskey regions, such as on the Kumtor Plateau, above Barskoon valley (KYR-38 and KYR-39) exhibit Middle Cretaceous ages of 108 ± 6 Ma and 110 ± 7 Ma, respectively and MTL values of 13.6 μm ($\sigma = 1.7$ μm) and 12.8 μm ($\sigma = 1.5$ μm).

The majority of Terskey Range samples were collected around Tashtarata peak, south of Kadji Sai village (Fig. 2). At lower elevations

Table 4
AFT age and length data: n is the number of counted grains; ρ_s, ρ_i, and ρ_d are the density of spontaneous, induced tracks and induced tracks in an external detector (ED) irradiated against a dosimeter glass. The ρ_d-values are interpolated values from regularly spaced glass dosimeters (IRMM-540). ρ_d is expressed as 10^5 tracks/cm^2; ρ_s and ρ_i are expressed as 10^6 tracks/cm^2. N_s, N_i, and N_d are the number of counted spontaneous, induced tracks and induced tracks in the ED. N_d is an interpolated value. P (χ^2) is the chi-squared probability that the dated grains have a constant ρ_s/ρ_i-ratio. An ζ-value of 253.1 ± 2.4 a·cm^2 was used for the calculation of the AFT age t(ζ) (in Ma). AFT length data are reported as a mean track length (l_m in μm) with standard deviation σ (in μm), obtained from the measurement of a number (n_l) of natural, horizontal confined tracks.

Sample	n	ρ_s (±1σ)	N_s	ρ_i (±1σ)	N_i	ρ_d (±1σ)	N_d	ρ_s/ρ_i	P (χ^2)	t(ζ)	l_m	n_l	σ
Zhetyzhol Range													
KAZ-01	30	3.793 (0.080)	2253	1.303 (0.047)	774	3.873 (0.083)	2181	3.034 ± 0.127	0.92	147.0 ± 7.0	12.4	100	1.6
KAZ-03	30	2.764 (0.068)	1642	0.840 (0.038)	499	3.870 (0.083)	2180	3.353 ± 0.171	1.00	162.2 ± 9.1	13.1	100	1.2
Trans-Ili Range													
ALMA03-3	30	0.745 (0.024)	942	0.485 (0.020)	614	3.668 (0.076)	2344	1.536 ± 0.080	0.99	70.9 ± 4.0	12.7	81	1.4
ALMA03-2	50	0.392 (0.013)	852	0.637 (0.017)	1365	3.672 (0.076)	2351	0.634 ± 0.028	0.99	29.4 ± 1.4	–	–	–
ALMA03-1	23	0.040 (0.006)	50	0.084 (0.008)	102	3.675 (0.076)	2358	0.494 ± 0.085	1.00	22.9 ± 4.0	–	–	–
Kungey Range													
TS-02	30	0.146 (0.008)	348	0.058 (0.005)	139	3.738 (0.108)	1196	2.734 ± 0.274	1.00	128.1 ± 13.4	–	–	–
TS-04	50	1.091 (0.023)	2281	0.393 (0.014)	820	3.751 (0.108)	1200	2.815 ± 0.115	0.99	132.3 ± 6.7	–	–	–
TS-06	30	2.927 (0.058)	2504	1.018 (0.034)	871	3.759 (0.108)	1203	2.919 ± 0.115	1.00	137.4 ± 6.8	12.4	100	1.5
TS-07	30	2.281 (0.059)	1518	0.829 (0.035)	547	4.157 (0.081)	2661	2.826 ± 0.141	0.96	147.0 ± 8.0	13.1	100	1.6
TS-08	30	2.059 (0.029)	4892	0.673 (0.017)	1599	3.771 (0.108)	1207	3.123 ± 0.090	0.95	147.3 ± 6.2	12.5	100	1.5
TS-09	20	3.952 (0.056)	5058	1.741 (0.037)	2229	4.011 (0.078)	2622	2.304 ± 0.059	0.57	115.9 ± 3.9	12.5	100	1.2
TS-10	30	2.492 (0.032)	5922	0.896 (0.019)	2130	3.785 (0.108)	1211	2.827 ± 0.072	0.89	134.0 ± 5.3	12.6	100	1.4
TS-11	30	1.965 (0.042)	2148	0.695 (0.025)	749	3.793 (0.108)	1214	2.910 ± 0.123	0.99	138.2 ± 7.2	12.3	73	1.5
TS-12	30	1.435 (0.044)	1058	0.586 (0.029)	418	4.152 (0.081)	2657	2.493 ± 0.144	1.00	129.7 ± 8.0	–	–	–
TS-13	30	3.736 (0.079)	2219	1.133 (0.044)	673	3.812 (0.109)	1220	3.418 ± 0.150	0.93	162.8 ± 8.7	12.4	100	1.3
TS-14	30	6.177 (0.128)	2348	1.957 (0.072)	744	3.818 (0.109)	1222	3.206 ± 0.135	0.97	153.1 ± 7.9	12.6	100	1.6
TS-18	30	2.273 (0.062)	1350	0.879 (0.038)	522	3.854 (0.110)	1233	2.609 ± 0.134	0.86	126.0 ± 7.5	13.0	96	1.7
Kyrgyz–Kungey Range transition (Kyzylkompol Ridge)													
TS-15	30	2.685 (0.056)	2297	0.881 (0.032)	754	3.823 (0.109)	1223	3.107 ± 0.130	0.94	148.6 ± 7.7	13.2	100	1.8
TS-16	30	1.585 (0.043)	1356	0.709 (0.029)	607	3.833 (0.109)	1226	2.299 ± 0.112	0.93	110.6 ± 6.3	12.9	100	1.4
TS-17	30	2.103 (0.050)	1799	0.875 (0.032)	749	3.848 (0.110)	1231	2.492 ± 0.108	0.91	120.2 ± 6.4	13.0	100	1.5
IK-01	20	1.613 (0.035)	2064	0.993 (0.028)	1271	3.708 (0.075)	2424	1.744 ± 0.062	0.18	81.3 ± 3.4	13.0	100	1.6
*IK-02**	*29*	*1.787 (0.031)*	*2534*	*1.365 (0.027)*	*2534*	*3.750 (0.080)*	*2180*	*1.319 ± 0.035*	*0.69*	*96.6 ± 3.4*	–	–	–
AI-88	15	4.102 (0.065)	3938	2.345 (0.049)	2251	4.033 (0.079)	2581	1.795 ± 0.047	0.21	91.0 ± 3.1	13.2	100	1.6
AI-90	15	4.773 (0.071)	4582	2.284 (0.049)	2193	3.823 (0.077)	2447	2.105 ± 0.055	0.38	101.0 ± 3.5	13.0	100	1.4
Terskey Range (Tashtarata)													
TS-19	6	1.515 (0.130)	135	0.719 (0.090)	64	4.147 (0.081)	2654	2.065 ± 0.313	0.96	107.5 ± 16.5	–	–	–
TS-20	60	0.939 (0.035)	714	0.779 (0.032)	592	3.869 (0.110)	1238	1.270 ± 0.071	1.00	61.9 ± 3.9	12.6	64	1.9
TS-22	19	0.754 (0.048)	250	0.576 (0.044)	173	3.887 (0.110)	1244	1.417 ± 0.140	0.97	69.3 ± 7.2	–	–	–
TS-23	30	0.901 (0.037)	600	0.637 (0.031)	433	3.893 (0.110)	1246	1.480 ± 0.093	0.98	72.0 ± 5.0	12.5	36	1.8
TS-24	30	1.218 (0.058)	445	0.614 (0.040)	232	4.137 (0.080)	2648	1.976 ± 0.160	1.00	102.6 ± 8.6	–	–	–
TS-26	45	0.129 (0.007)	371	0.088 (0.006)	254	4.127 (0.080)	2641	1.510 ± 0.123	1.00	78.4 ± 6.6	–	–	–
TS-27	30	1.183 (0.034)	1170	0.533 (0.023)	529	3.692 (0.075)	2397	2.144 ± 0.112	0.99	99.4 ± 5.7	11.7	28	1.4
TS-28	6	1.280 (0.096)	177	0.830 (0.081)	105	3.688 (0.075)	2392	1.849 ± 0.228	0.53	85.7 ± 10.7	–	–	–
AI-01	31	0.940 (0.030)	1130	0.702 (0.024)	850	3.715 (0.075)	2438	1.370 ± 0.062	0.42	64.1 ± 3.2	–	–	–
AI-04	30	0.727 (0.022)	1085	0.497 (0.019)	722	3.716 (0.075)	2440	1.459 ± 0.070	0.92	68.2 ± 3.6	–	–	–
AI-05	60	0.052 (0.004)	136	0.496 (0.014)	1291	3.717 (0.075)	2442	0.106 ± 0.010	1.00	5.0 ± 0.5	–	–	–
AI-09	3	2.050 (0.145)	199	1.422 (0.124)	132	4.033 (0.079)	2581	1.357 ± 0.152	0.28	68.9 ± 7.9	–	–	–
KYR-33	5	0.998 (0.094)	112	0.415 (0.063)	44	3.970 (0.079)	2541	2.325 ± 0.414	0.85	115.8 ± 20.8	–	–	–
Terskey Range (Barskoon)													
KYR-35	50	0.246 (0.009)	786	0.308 (0.010)	986	3.311 (0.074)	1986	0.913 ± 0.044	0.25	38.1 ± 2.0	–	–	–
KYR-38	50	0.613 (0.017)	1354	0.293 (0.012)	646	4.133 (0.079)	2708	2.090 ± 0.100	0.99	108.4 ± 5.7	13.6	100	1.7
KYR-39	20	1.869 (0.054)	1182	0.763 (0.035)	473	3.389 (0.075)	2028	2.589 ± 0.414	0.49	110.1 ± 6.6	12.8	27	1.5
KYR-42	30	0.663 (0.021)	984	1.735 (0.034)	2684	3.392 (0.075)	2035	0.411 ± 0.015	0.20	17.6 ± 0.8	–	–	–
Terskey Range (Karakol)													
IK-11	35	2.048 (0.072)	820	0.827 (0.046)	320	3.924 (0.082)	2296	2.640 ± 0.174	1.00	129.8 ± 9.1	–	–	–
IK-12	3	0.117 (0.032)	13	0.147 (0.037)	16	3.711 (0.075)	2429	0.825 ± 0.308	0.88	38.6 ± 14.4	–	–	–
IK-13	45	0.306 (0.010)	882	0.529 (0.014)	1523	3.713 (0.075)	2433	0.560 ± 0.024	0.56	26.3 ± 1.3	–	–	–
AI-27	25	1.511 (0.039)	1469	0.684 (0.026)	672	4.245 (0.105)	1634	2.250 ± 0.105	0.99	122.6 ± 6.7	–	–	–
Terskey Range (other locations)													
AI-33	3	1.458 (0.140)	109	0.391 (0.071)	30	4.249 (0.082)	2718	3.739 ± 0.771	0.60	198.0 ± 41.0	–	–	–
*IK-07**	*5*	*2.166 (0.025)*	*99*	*2.181 (0.130)*	*98*	*3.830 (0.080)*	*2241*	*1.320 ± 0.085*	*0.33*	*75.2 ± 11.0*	–	–	–

on the north-verging flanks, Middle Cretaceous ages of 116 ± 21 Ma to 99 ± 6 Ma are found, while samples from higher elevations generally have Late Cretaceous ages between 86 ± 11 Ma and 62 ± 4 Ma (Table 4, Fig. 5). The inverted age–elevation relationship for these samples might imply the presence of down-faulted blocks on these northern Terskey slopes. Length data is scarce for this region. A similar age of 71 ± 4 Ma was also calculated for sample ALMA3-03 from the higher northern flanks of the Trans-Ili Range in Kazakhstan, north of the Issyk-Kul Basin and the Kungey Range. An MTL value of 12.7 μm was measured (σ = 1.4 μm) for the latter sample.

The two other samples from the Trans-Ili Range, collected at lower elevations, record Oligocene–Miocene AFT ages of 29 ± 1 Ma and

23 ± 4 Ma. Similar Oligocene–Miocene ages are also found in the Terskey Range, such as in the lower sections of the Barskoon Valley transect (KYR-42 and KYR-35) with ages of 38 ± 2 to 18 ± 1 Ma and at the eastern end of the Range (IK-13 and IK-12) with ages of 39 ± 14 to 26 ± 1 Ma. Finally, in the southern flank of Tashtarata peak (Terskey Range sample AI-05), a Pliocene age of 5.0 ± 0.5 Ma was obtained (Table 4, Fig. 5). Due to low spontaneous track densities for this youngest age cluster, no AFT length date was acquired.

For a limited amount of the apatite samples, AHe ages were obtained as well (Table 5, Fig. 5). For some apatites from the older AFT age groups and/or apatites with high spontaneous track densities, anomalously high apparent AHe ages were found. When the AHe age of a sample is higher than its corresponding AFT age, it is considered to exhibit an "anomalously high AHe age" as closure temperatures for the AFT system should be higher than for the AHe system. This "He-anomaly" constitutes a well-known phenomenon in apatite thermochronology (Green and Duddy, 2006; Flowers and Kelley, 2011). In most cases it can be associated with excess ^{4}He produced by inclusions, with ^{4}He implantation from adjacent U-rich minerals (Spiegel et al., 2009), or with radiation damage and He-trapping (Shuster et al., 2006). The latter process is especially applicable to old and/or U-rich apatites in which case a high spontaneous latent track density can provide an intricate network of He-traps, inhibiting further He diffusion.

In our data, anomalously high AHe ages (italic in Table 5) are found for the Jurassic Zhetyzhol Range samples (KAZ-01 and KAZ-03). In most cases these "anomalous ages" cannot be used for further discussion or thermal history modeling. However, some of the old AHe ages are only slightly older than the corresponding AFT ages and actually overlap within analytical uncertainty. In these instances we can state that AHe and AFT ages are near-identical, and cooling through AFT and AHe closure temperatures most probably occurred rapidly. An example of this is sample TS-17 (Table 5, Fig. 5) with near-identical AHe and AFT ages of 120 ± 6 Ma and 123 ± 8 Ma, respectively. Other samples show normal AFT–AHe relationships where e.g. Mesozoic AFT ages are somewhat older than their AHe counterparts. As an illustration of the latter case, Terskey Range sample KYR-38 has an apparent Middle Cretaceous AFT age of 108 ± 6 Ma, and a Late Cretaceous AHe age of 85 ± 5 Ma. This could point to a more moderate Mesozoic cooling rate for this sample as compared to e.g. TS-17. For two samples with Oligocene–Miocene AFT ages (bold in Table 5), AHe ages were obtained as well and these further constrain the Late Cenozoic formation of the modern Kyrgyz Tien Shan orogen. Sample ALMA3-01 (Trans-Ili Range) with an Early Miocene AFT age of 23 ± 4 Ma, has a Middle Miocene AHe age of 15 ± 1 Ma, and sample IK-13 from the eastern section of the Terskey Range has a similar AHe age of 11 ± 1 Ma (as compared to its AFT age of 39 ± 14 Ma).

The AFT and AHe age groups described above have been widely recognized throughout several areas of the Tien Shan orogen, both in the Kyrgyz and Chinese segments and attest to widespread, regional Meso-Cenozoic reactivation and exhumation events. The oldest AFT ages in the Tien Shan are Triassic–Early Jurassic. These oldest apatites mainly occur in the detrital record, such as in the Ferghana, Alai and Naryn basins in the Southern and Middle Kyrgyz Tien Shan (De Grave et al., 2011b; Glorie et al., 2011b), in similar intramontane basins in the Chinese Tien Shan (Dumitru et al., 2001), and in the Junggar (Hendrix et al., 1994) and the Tarim (Sobel and Dumitru, 1997) foreland basins. Sporadically these ages are found preserved in the exhumed basement as well. In the Kyrgyz Tien Shan this is most outspoken in the Song-Kul area (De Grave et al., 2011a) and for one location in the Atbashi Range (Glorie et al., 2011b). In the southern Chinese Tien Shan, this age group is found locally in the South Borohoro and Erbin Range (Dumitru et al., 2001; Jolivet et al., 2010).

Late Jurassic and Cretaceous basement and detrital AFT ages compile the bulk of the available Tien Shan thermochronometric data set. This data comes from studies in the Northern and Middle Kyrgyz Tien Shan (Bullen et al., 2001; Sobel et al., 2006b; Glorie et al., 2010; De Grave et al., 2011a), the Southern Kyrgyz Tien Shan (De Grave et al., 2011b; Glorie et al., 2011b), several areas in the Chinese Tien Shan (Dumitru et al., 2001; Wang et al., 2009; Jolivet et al., 2010) and in the Tarim and Junggar basins and adjoining basement blocks (Hendrix et al., 1994; Sobel and Dumitru, 1997; Sobel et al., 2006a; Zhang et al., 2009, 2011).

The building of the modern Tien Shan belt is accompanied by renewed exhumation and associated cooling of the composing basement blocks. This most recent evolution of the Tien Shan is recorded in the basement and detrital thermochronometry archive and shows that incipient deformation began in the Oligocene, and that exhumation was widespread in the orogen from the Miocene onwards (Hendrix et al., 1994; Sobel and Dumitru, 1997; Bullen et al., 2001; Dumitru et al., 2001; Sobel et al., 2006a; Wang et al., 2009; Glorie et al., 2010; Jolivet et al., 2010; Glorie et al., 2011b; De Grave et al., 2011b). Oligocene and Miocene cooling ages are recognized in the Pamirs and Karakoram as well (e.g. Leloup et al., 2011; Schmidt et al., 2011).

The Mesozoic exhumation and denudation episodes in the Tien Shan are often attributed to the influence of far-field tectonic effects (De Grave et al., 2007). During the Mesozoic, a multi-stage orogeny affected the southern fringes of the Eurasian continent as a consequence of progressive closure of the Tethyan Ocean basins and the punctuated collisions of peri-Gondwanan blocks (Golonka, 2004). Accretion of these Cimmerian blocks invoked tectonic reactivation of several mobile belts in the CAOB edifice. This protracted Cimmerian orogeny reactivated several major inherited structures in the ancestral Tien Shan, creating a multi-stage Mesozoic Tien Shan mountain belt (e.g. Allen and Vincent, 1997). Similar to the Late Triassic collision of the Qiangtang block as discussed in a previous section, the collision of the current Tibetan Lhasa block in the Late Jurassic–Early Cretaceous (~150–120 Ma; Kapp et al., 2007; Leier et al., 2007), and that of the Kohistan–Dras arc, and the Karakoram block in the Late Cretaceous (~90–70 Ma; Schwab et al., 2004) with Eurasia exerted distant tectonic effects on the Tien Shan (e.g. Otto, 1997; Dumitru et al., 2001; Jolivet et al., 2010; De Grave et al., 2011b). Differential uplift within the orogen created several intramontane basins (e.g.

Table 5
Apatite (U–Th–Sm)/He dating results. Concentrations for U, Th and Sm are listed in ppm, the ^{4}He concentration is in nmol/μg. The mass, m, of the apatite grains is in μg. F_T is the α-ejection correction factor (Farley, 2002). Average sample values are given (based on at least two reproducible aliquots). AFT ages are listed for comparison. In italic: anomalously high AHe ages with respect to the AFT age; in bold: reset, i.e. Late Cenozoic, AHe ages.

Sample	U	Th	Sm	Th/U	He	m	F_T	t (AHe)	t (AFT)
KAZ-01	19.2	58.8	104.7	5.6	32.4	2.9	0.58	*296.3 ± 17.8 Ma*	147.0 ± 7.0 Ma
KAZ-03	28.6	67.8	76.8	2.4	28.3	4.0	0.61	*190.6 ± 11.5 Ma*	162.2 ± 9.1 Ma
ALMA03-1	10.6	33.0	87.1	2.8	0.8	2.6	0.57	**14.6 ± 0.9 Ma**	22.9 ± 4.0 Ma
TS-06	62.2	109.4	45.6	1.8	43.4	3.2	0.57	*159.9 ± 9.6 Ma*	137.4 ± 6.8 Ma
TS-13	34.5	105.4	54.1	3.2	67.9	2.3	0.65	*312.3 ± 16.7 Ma*	162.8 ± 8.7 Ma
TS-15	20.6	46.5	74.2	2.3	13.4	10.1	0.70	111.6 ± 6.7 Ma	148.6 ± 7.7 Ma
TS-17	67.2	104.0	115.0	1.6	32.5	3.0	0.55	122.5 ± 7.6 Ma	120.2 ± 6.4 Ma
TS-26	7.7	25.2	120.9	3.2	9.0	1.4	0.60	*183.5 ± 11.0 Ma*	78.4 ± 6.6 Ma
KYR-38	9.3	20.2	196.5	2.4	4.3	1.7	0.62	85.0 ± 5.1 Ma	108.4 ± 5.7 Ma
IK-03	33.1	139.4	70.9	4.0	45.7	4.5	0.62	186.3 ± 11.2 Ma	–
IK-13	19.2	102.4	31.8	5.4	1.8	7.9	0.69	**11.4 ± 0.7 Ma**	38.6 ± 14.4 Ma

Issyk-Kul Basin) and denudation of the developing mountain ranges exhumed the Tien Shan crystalline basement. Consequently this basement was cooled as reflected in the thermochronometric record. Sediments, also contain these cooling age signals in their detrital archive and were deposited in both the embryonic intramontane basins and the larger foreland basins (Graham et al., 1993). From sedimentologic and provenance analyses Hendrix (2000) concluded that the Junggar and Tarim forelands were effectively separated by advancing Mesozoic Tien Shan mountain ranges.

Late Jurassic and Cretaceous AFT and AHe ages are prevalent in the basement blocks surrounding the Issyk-Kul Basin (Fig. 5). They reflect the exhumation and cooling of the basement at the time of Mesozoic deformation in the Tien Shan. Although there is some spread, there is a clear distinction between the exhumation ages and rates for the individual ranges that characterize the Issyk-Kul area. Several topographic profiles across the basin are shown in Fig. 6; other results are in Fig. 5. AFT and AHe ages for the granitoid samples along these profiles are indicated. Late Jurassic ages are found in the Zhetizhol Range and the eastern section of the Kungey Range (Figs. 5 and 6). In the central and western sections of the Kungey Range, both on the southern and northern flanks, and along the Chon Kemin valley, mainly Early Cretaceous cooling ages are preserved. At the junction zone of the Kungey, Terskey and Kyrgyz Range, near Orto-Tokoj and Kyzylkompol Ridge, somewhat younger, Middle Cretaceous ages dominate. Similar Middle Cretaceous ages are also found at higher elevations in the Terskey Range (e.g. Kumtor Plateau). At lower elevations of the Tashtarata section, clearly younger ages are found. Here, Late Cretaceous ages account for the bulk of the data. Finally, Cenozoic ages are concentrated in fault zones in the Terskey block (e.g. Barskoon area, Terskey fault) and at low elevation in the north-verging flanks of Trans-Ili Range (Karakunug–Zaili fault), just across the border into Kazakhstan.

This indicates that the crystalline basement of the sampled areas in the Zhetizhol Range and the eastern section of the Kungey Range was exhumed to depths within the apatite PAZ (APAZ) by the Late Jurassic

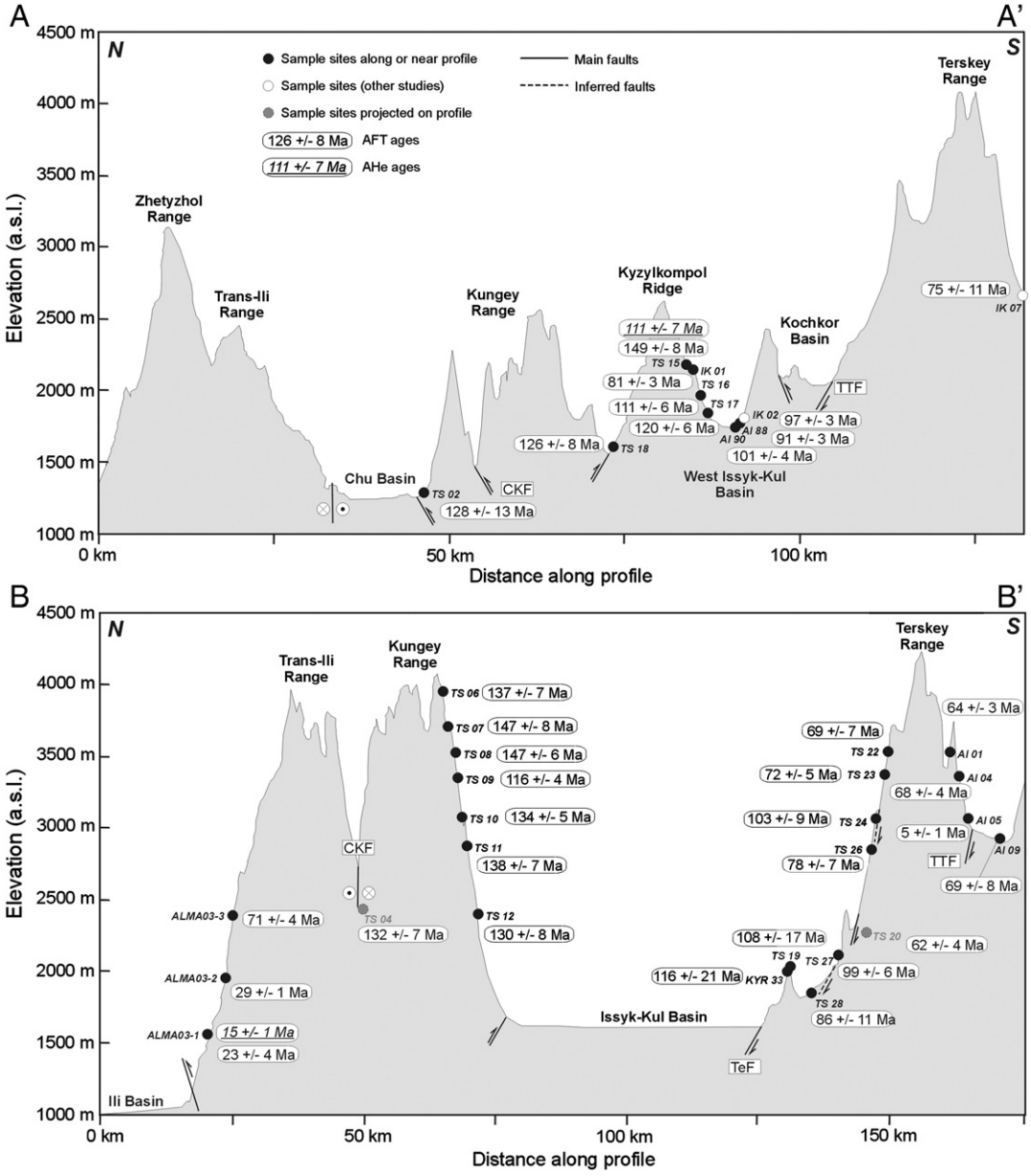

Fig. 6. Topographic profiles across the Issyk-Kul Basin (A–A′, B–B′, C–C′ and D–D′, see Fig. 2 for locations) with indication of apatite fission-track (AFT) and apatite (U–Th–Sm)/He (AHe) ages. Sample sites from our previous studies (Glorie et al., 2010, 2011b; De Grave et al., 2011a) where similar ages are found are indicated as white circles. See text for discussion.

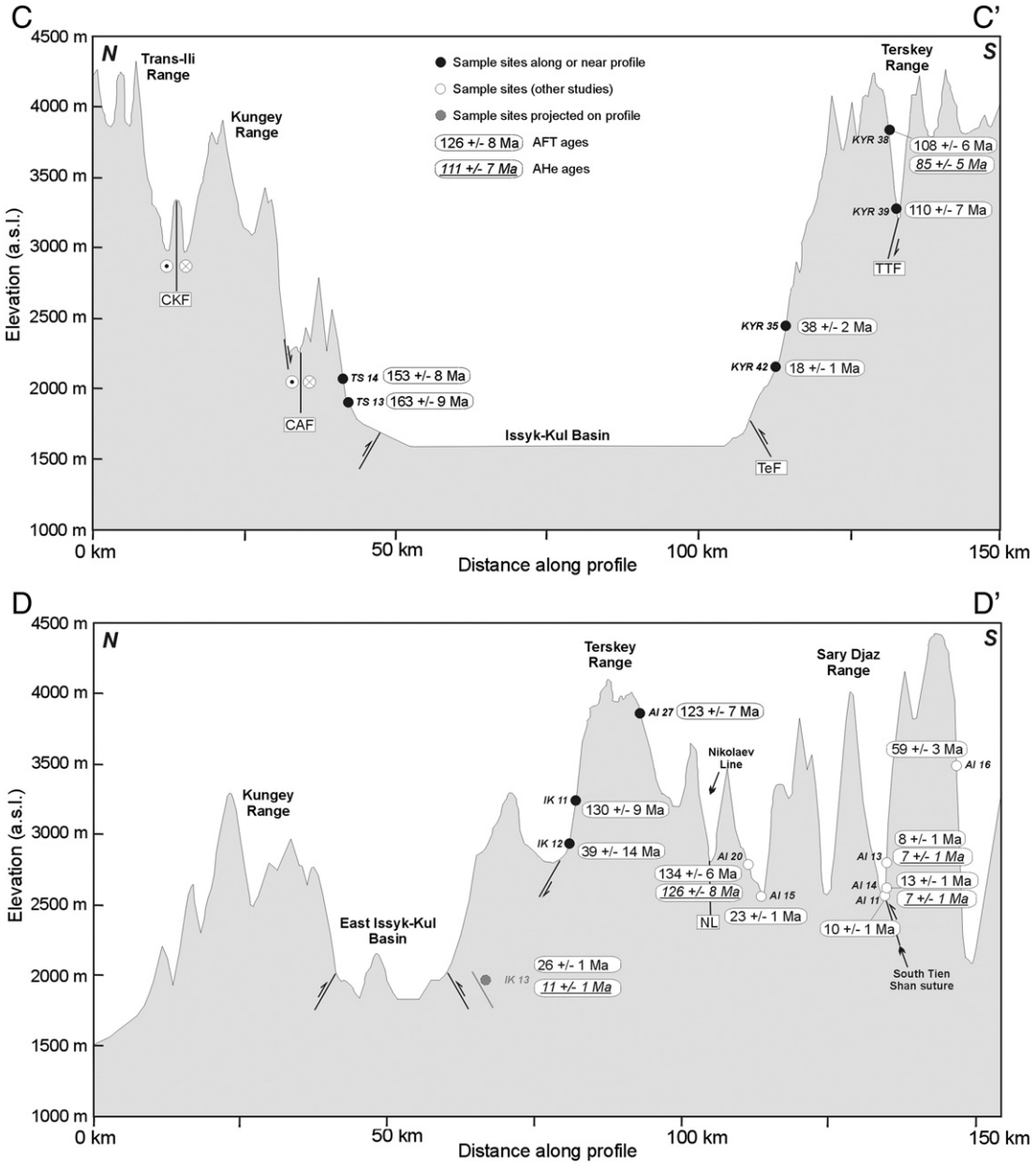

Fig. 6 (*continued*).

and that subsequent accumulated denudation as response to Cretaceous and Cenozoic tectonic activity in the Tien Shan brought these rocks to their present outcrop positions. The somewhat younger ages in the western section of the Kungey Range demonstrate that this part of the Issyk-Kul basement was to some extent exhumed more rapidly or in other words, deeper palaeo-levels have now been exposed as a consequence of more profound Cretaceous and Cenozoic denudation. The Middle Cretaceous ages at the Kungey, Terskey and Kyrgyz Range junction around Orto-Tokoj and the Kyzylkompol Ridge, and preserved at higher elevations in the Terskey block (e.g. Kumtor Plateau) in their turn bear witness to even higher degrees of basement exhumation. The northern flank of the central Terskey Range (Tashtarata) that predominantly yields samples with Late Cretaceous cooling ages, suggests that this section of the Issyk-Kul basement was subjected to intense denudation, restricted to the latest Mesozoic and in the Cenozoic. Late Cenozoic ages occur in distinct zones along the current Zaili (i.e. Trans-Ili) and Karakunug fault zones in the Trans-Ili Range and along the Terskey fault (Fig. 7). These indicate that Late Cenozoic activity along these fault zones is responsible for the growth of the mountain ranges and that intense denudation in these fault dominated areas has been intense enough to exhume basement blocks that were below the APAZ prior to the onset of these movements. Deep incision and associated intense denudation of crystalline basement, concentrated in and near reactivated fault zones in the Tien Shan edifice have been described previously by e.g. Bullen et al. (2001), Sobel et al. (2006b), Jolivet et al. (2010), and Glorie et al. (2011b). Hence, during several phases of reactivation, deformation is mainly concentrated along inherited zones of weakness in the Tien Shan crust (e.g. Allen and Vincent, 1997; Poupinet et al., 2002).

From the profiles shown in Fig. 6, it is also clear that where vertical sections were sampled in high resolution, such as along the Orto-Koi-Suu valley in the Kungey Range, samples are characterized by near-identical ages for the entire vertical section. In the latter case, Late Jurassic–Early Cretaceous AFT ages occur over an elevation difference of almost 2 km. This indicates that over the entire section more or less the same palaeo-surface is sampled and that hence

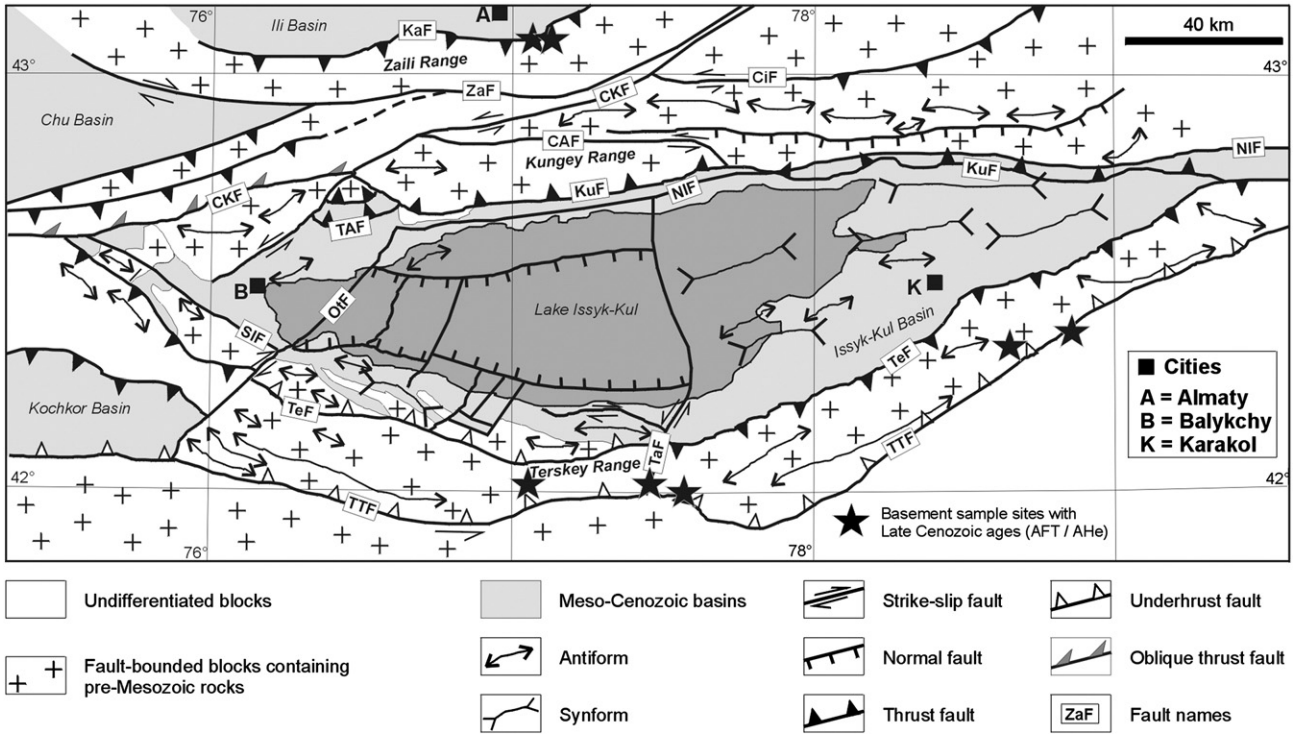

Fig. 7. Schematic map of active tectonic structures in the Issyk-Kul Basin area (based on Buslov et al., 2003a). Samples for which Late Cenozoic low-T thermocronometric results are found are located on or close to these active structures.

to some extent basement block tilting is involved. This explains that over a section of 2 km no younger samples of an exhumed palaeo-APAZ were found at the base of the vertical section. At the opposite side of the basin, in the Terskey Range profile, a similar, albeit more complex tilting pattern can be recognized. In the North-facing flank, on top of Tashtarata peak, and at higher elevations in the south-verging part of the range, Late Cretaceous ages are found. At the base of the south flank a young age of 5 Ma was obtained, which indicates that this part of the range was deeply incised by the Terskey fault system. Some older Cretaceous ages on the north flank, in particular at low elevations, might represent older basement sections preserved in down-faulted blocks.

3.4. Thermal history models

From these Cenozoic apatites, no AFT length data is available due to low spontaneous track densities. No ^{252}Cf or heavy ion irradiation was performed and hence the amount of confined tracks was insignificant. For most of the Mesozoic apatites, AFT length data is provided (Table 4, Fig. 5) and thermal history modeling using the HeFTy software (Ketcham, 2005) was carried out on all of these. Where applicable and when AHe ages were not anomalously high, AHe data was also used in the numerical modeling. For all the basement-cored mountain ranges surrounding the Issyk-Kul Basin one or more representative thermal history models are shown in Fig. 8 (good fit envelopes). The models for the Middle to Late Jurassic samples from the Zhetizhol Range (that represent the oldest apparent AFT ages in the study area) indicate an episode of rapid Early to Middle Jurassic (~180–160 Ma) cooling. We interpret this cooling as exhumation of the Zhetizhol basement during an early phase of Cimmerian reactivation, possibly resulting from the accretion–collision of Qiangtang in the Triassic–earliest Jurassic (e.g. Pullen et al., 2008). Alternatively, some of the Middle Mesozoic reactivation in the Tien Shan (particularly the northern and northeastern sections) might be attributed to distant effects of the Mongol–Okhotsk orogeny (e.g. Jolivet et al., 2010). This orogeny most likely affected areas of the CAOB to the north (present-day co-ordinates) of the Tien Shan. It is envisaged that early construction of the Mongol–Okhotsk orogen commenced in the Early Jurassic (~180–170 Ma) between the colliding orogenic rim of Siberia with the composite North China–Mongolia continent (or Amurian continent) as closure of the intervening Mongol–Okhotsk Ocean progressed (e.g. Cogné et al., 2005; Metelkin et al., 2010). In the Mongolian Altai and the Siberian Altai–Sayan Mountains, the Mongol–Okhotsk orogeny is often cited as a main driving force for the Mesozoic reactivation of this part of the CAOB. This is observed in the low-temperature thermochronometric data for this region (e.g. De Grave and Van den haute, 2002; Jolivet et al., 2007, 2009; Vassallo et al., 2007; De Grave et al., 2008; 2009; 2011c; Glorie et al., 2012).

While it can be hazardous to interpret Late Cenozoic cooling merely from thermal history modeling alone (Ketcham et al., 1999), there is a lot of independent geological evidence in the Issyk-Kul area to state that Late Cenozoic basement cooling is very plausible. The occurrence of both Oligocene and Mio-Pliocene AFT and AHe ages in our study area is an important argument. The lacustrine sedimentary sequences in Issyk-Kul Basin (and other nearby basins) further show the presence of Oligocene and thick Mio-Pliocene coarse clastic deposits (e.g. Kyrgyz Suite, Issyk-Kul or Chreyskaya Suite, and Chapeldak Suite sediments) associated with erosion of the growing adjoining mountain ranges (e.g. Cobbold et al., 1994). Therefore the last phase of modest cooling seen in the Zhetizhol thermal history models might be an expression of this. This final cooling event, that brought the investigated samples from upper APAZ temperatures — lower AFT retention zone temperatures to current ambient conditions at outcrop position, seems to start from the Oligocene–Early Miocene (~30–25 Ma). This might reflect the onset of current mountain building and related denudation in the northern Tien Shan. The modern Tien Shan orogen is developing as a distant response to India–Eurasia convergence, a main driving force that affects the CAOB as a whole (e.g. De Grave et al., 2007).

Very similar thermal history models were obtained from the Kungey Range samples (Fig. 8). Here, a Jurassic rapid cooling event is interpreted as the Jurassic exhumation of its basement. Compared to the Zhetizhol models, where this cooling is modeled between ~180 and 160 Ma, the Kungey samples exhibit wider good-fit tT-path envelopes for the Jurassic

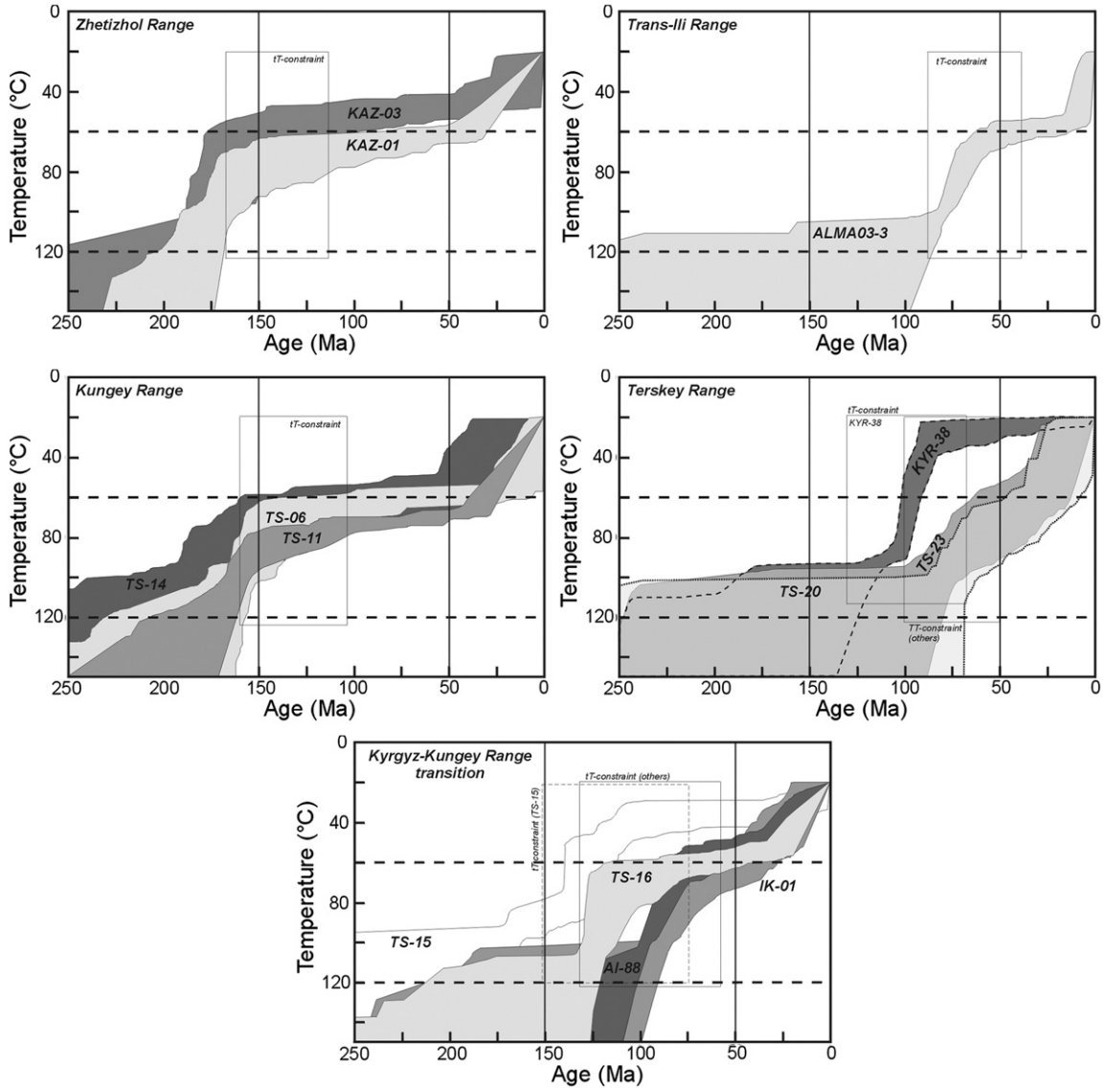

Fig. 8. Representative thermal history models (using HeFTy, Ketcham, 2005) from selected sample sites.

event, and cooling is modeled here between about ~180–140 Ma. After Late Mesozoic–Early Cenozoic stabilization, also the Kungey models exhibit an additional Late Cenozoic cooling event. Here as well there is some more spread in relation to the Zhetizhol samples, but this latest cooling also seems to initiate roughly around 25 Ma in the Kungey Range. The interpretation of these thermal history models is hence identical to that of Zhetizhol outlined above. In between the Mesozoic and potential Late Cenozoic rapid cooling event, a period of Late Mesozoic–Early Cenozoic stability can be associated with the development of a contemporaneous peneplanation surface of which remnants are found at several locations in the Kyrgyz Tien Shan (e.g. Mikolaichuk et al., 2003).

The thermal history models for the samples near the western edge of the Issyk-Kul Basin (Orto-Tokoj region) show more scatter. As implied by the younger AFT ages, the cooling history of this part of the basement points to an important Cretaceous event (Fig. 8). Most of the samples in this area indicate a modeled Late Cretaceous rapid cooling phase: between about 100 and 75 Ma for samples IK-01 and AI-88, and around 125–100 Ma for TS-16. Sample TS-15 shows a somewhat earlier initiation of cooling in the Early Cretaceous. As mentioned, the Cretaceous Period is characterized by punctuated collision–accretion events on the southern Eurasia margin: Lhasa in the Early Cretaceous (Kapp et al., 2007; Leier et al., 2007), and the Kohistan–Dras arc, and the Karakoram block in the Late Cretaceous (~70–90 Ma; e.g. Schwab et al., 2004). We interpret the Cretaceous cooling in the Tien Shan basement in northern Kyrgyzstan as response to differential denudation of basement blocks in this framework of renewed tectonic reactivation. While the tT paths for sample TS-15 show that the sample reached surface temperatures already immediately after cessation of Mesozoic cooling (~100 Ma), the other thermal histories for this area suggest a renewed, Late Cenozoic cooling starting around 25 Ma as also implied by the thermal history models for the Zhetizhol and Kungey samples.

For samples of the Trans-Ili Range, only the uppermost Late Cretaceous sample could be modeled. The Miocene AFT samples did not contain enough confined tracks. The thermal history model for sample ALMA3-03 shows great similarity with samples from the Orto-Tokoj region, especially IK-01 and AI-88. Sample ALMA3-03 was affected by rapid Late Cretaceous cooling (~75 Ma) which can be attributed to the same aforementioned Cretaceous Cimmerian driving forces. More outspoken than the comparable thermal histories, ALMA3-03 exhibits a distinct Late Cenozoic cooling event as well. The model reveals that onset of this cooling was around 15–20 Ma, and this coincides well with the Oligocene–Early Miocene AFT ages of the Trans-Ili samples taken down section.

As mentioned, several thermochronological studies across the entire Tien Shan have shown these Late Cenozoic exhumation ages of the orogen (Hendrix et al., 1994; Sobel and Dumitru, 1997; Bullen et al., 2001; Dumitru et al., 2001; Sobel et al., 2006a; Wang et al., 2009; Glorie et al., 2010; Jolivet et al., 2010; Glorie et al., 2011b; De Grave et al., 2011b). Miocene–Pliocene building of the modern Tien Shan is also inferred from several other lines of evidence, such as magnetostratigraphy for example. These analyses performed on Neogene sedimentary sequences in the Tien Shan and adjoining basins have revealed pulsed denudation or episodic exhumation of the Tien Shan through the Miocene, Pliocene, and Pleistocene (e.g. Bullen et al., 2001; Sun et al., 2007; Ji et al., 2008; Charreau et al., 2009; Li et al., 2011a, 2011b, amongst others).

For the Terskey Range also a limited amount of samples were modeled due to low confined track densities and a consequential lack of length data. Thermal histories from the Late Cretaceous Tashtarata area (TS-20, TS-23) yield a straightforward cooling history from the Late Cretaceous to the present. Older samples from the Kumtor plateau on top of the Terskey Range (KYR-38) show a more rapid cooling in the Late Cretaceous up to ambient temperatures. No further cooling is then observed in this model. This is corroborated by the presence of a well-defined Late Cretaceous–Palaeogene peneplanation surface on the plateau. An overview of the tectonic events affecting the Tien Shan basement in relation to the ages obtained from that basement using various low-temperature dating techniques is given in Fig. 9.

4. Conclusions

The Issyk-Kul Basin represents one of the largest intramontane basins in the entire Tien Shan orogen and its basement records several Meso-Cenozoic tectonic events that transpired in the Tien Shan. The basin formed on the Late Precambrian–Palaeozoic basement of the Kyrgyz Northern Tien Shan (NTS). This NTS unit is a composite of several microcontinents that are wedged between two major CAOB blocks, i.e. Palaeo-Kazakhstan and Tarim. During the Early Palaeozoic, a continental magmatic arc was built on the NTS and the related granitoid plutons were the major targets for this multi-method chronologic study. This multi-method approach with the application of zircon U/Pb (ZUPb), K-feldspar $^{40}Ar/^{39}Ar$, titanite fission track (TFT), apatite fission track (AFT) and apatite (U–Th–Sm)/He (AHe) dating and thermal history modeling, enables us to reconstruct the thermotectonic history of the Issyk-Kul basement as itemized below.

1) Late Ordovician–Silurian (456–420 Ma) ZUPb crystallization ages were obtained for the Issyk-Kul granitoids. The youngest ages are found in the northern section of the Issyk-Kul basement. These results indicate an important phase of Early Palaeozoic granitoid magmatism, related to the closure of the Terskey Ocean (as part of the larger Palaeo-Asian Ocean) and the subsequent building of the NTS continental magmatic arc. The youngest (~420 Ma) ZUPb ages might be related with a Late Silurian period of back-arc extension.
2) During the Late Palaeozoic, Tarim and Palaeo-Kazakhstan eventually collided as the intervening oceanic basin, the Turkestan Ocean, was closed and the ancestral Tien Shan was formed. Smaller volumes of post-collisional granites constrain this collision to the Late Carboniferous–Early Permian.
3) Late Carboniferous–Triassic (~310–220 Ma) TFT and K-feldspar $^{40}Ar/^{39}Ar$ ages were obtained which constrain a first phase of tectonically induced cooling preserved in the basement of the Issyk-Kul Basin. During this period, the Tien Shan basement structures were subjected to intensive transpressional and transtensional reactivation as response to enduring Tarim–Palaeo-Kazakhstan convergence. Furthermore, the adjacent Tarim basement started to subside, providing a base-level drop and accommodation space for sediments derived from Tien Shan source areas. This would have invoked denudation and hence cooling of the Tien Shan basement.
4) Most AFT and AHe ages for the Issyk-Kul basement can be grouped in a Late Jurassic–Early Cretaceous (~150–130 Ma), a Middle Cretaceous (~110–90 Ma) and Late Cretaceous (~75–65 Ma) age cluster. Early Jurassic (~200–175 Ma) K-feldspar $^{40}Ar/^{39}Ar$ and TFT ages

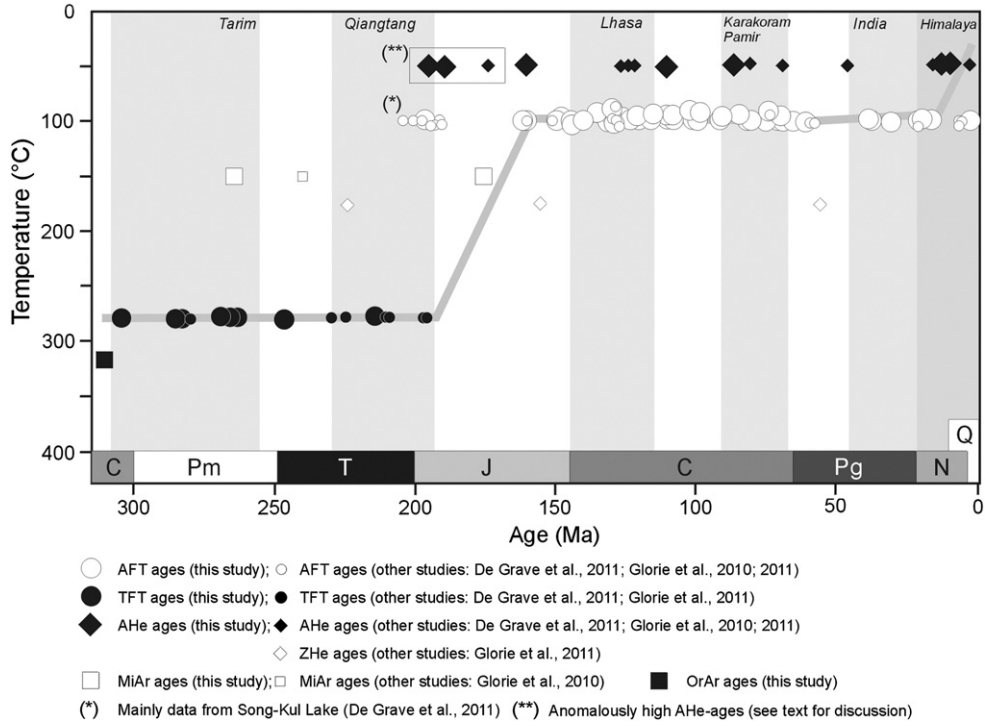

Fig. 9. Multi-method low-temperature thermochronometry of the Issyk-Kul basement in the Northern Kyrgyz Tien Shan: overview of the available ages by apatite fission-track dating (AFT), apatite (U–Th–Sm)/He dating (AHe), microcline $^{40}Ar/^{39}Ar$ dating (MiAr), orthoclase $^{40}Ar/^{39}Ar$ dating (OrAr), titanite fission-track dating (TFT), and zircon (U–Th–Sm)/He dating (ZHe). Main accretion–collision events shaping the Tien Shan basement over time are schematically shown: Permian Tarim collision, Mesozoic "Cimmerian" collisions (Qiangtang, Lhasa, Karakoram–"Pamir") and the Cenozoic India–Eurasia collision.

were obtained as well. These ages can be linked to far-field effects of Late Triassic–Cretaceous accretion of peri-Gondwanan blocks (Qiangtang, Lhasa, Karakoram) from the Tethyan realm to the Eurasian margin. These caused reactivation of Tien Shan basement structures and led to denudation/exhumation and hence cooling of crystalline basement rocks.

5) Although there is some spread, there is a clear distinction between the Mesozoic exhumation ages and rates for the individual mountain ranges and associated basement blocks that characterize the Issyk-Kul area. In the central and western sections of the Kungey Range, mainly Early Cretaceous cooling ages are preserved. At the junction zone of the Kungey, Terskey and Kyrgyz Range, and at higher elevations in the Terskey Range (e.g. Kumtor Plateau), Middle Cretaceous ages dominate. At lower elevation, especially on the north-facing slopes of the Terskey Range, Late Cretaceous ages are prevalent. Hence, Mesozoic denudation was more intensive at the southern margin of the Issyk-Kul Basin.
6) At several locations along important fault-zones such as the Trans-Terskey Fault and the Karakunug–Zaili Fault, Oligocene–Pliocene AFT and AHe ages (~35–5 Ma) were obtained. These ages can be linked with renewed reactivation and final building of the Tien Shan, as a result of stress-propagation from the India–Eurasia collision. The occurrence of these ages within the aforementioned inherited fault zones indicates that Cenozoic mountain building was at least partly controlled by fault-reactivation.
7) The AFT (and to a lesser extent AHe) ages furthermore suggest that during Cenozoic reactivation, the Kungey and Terskey Range basement blocks were tilted towards the Issyk-Kul basin and provoked further flexural basin subsidence.

Acknowledgments

The authors are supported by grants of the Fund for Scientific Research — Flanders (FWO, Belgium) (JDG) and the Institute for the Promotion of Innovation through Science and Technology in Flanders (IWT-Vlaanderen) (SG). This research was co-funded by Ghent University (BOF — bilateral project 01SB1309). We are indebted to Dr. Guido Vittiglio and Dr. Peter Vermaercke for help with irradiations and neutron dosimetry at the Belgian Nuclear Research Centre in Mol (SCK-CEN, BR1 facility) and to Prof. Dr. Frank Vanhaecke and Dr. Andrei Izmer for use of the ICP-MS infrastructure at the Atomic and Mass Spectrometry unit (Dept. Analytical Chemistry, UGent). Dr. James Metcalfe is acknowledged for his help during the Ar-analyses at Stanford and Prof. Eric Van Ranst for performing feldspar XRD analyses at the Solid Science Dept. (UGent). Several colleagues and students assisted during the various field campaigns in Kyrgyzstan, for which we are very grateful. Two anonymous reviewers provided constructive remarks which helped to improve our paper and we take this opportunity to thank them for their input.

References

Abdrakhmatov, K.Y., Djanuzakov, K.D., Delvaux, D., 2002. Active tectonics and seismic hazard of the Issyk-Kul basin in the Kyrgyz Tian-Shan. In: Klerkx, J., Imanackunov, B. (Eds.), Lake Issyk-Kul: Its Natural Environment. Kluwer Academic Publishers, Dordrecht, pp. 147–160.

Abrajevitch, A., Van der Voo, R., Bazhenov, M.L., Levashova, N.M., McCausland, P.J.A., 2008. The role of the Kazakhstan orocline in the late Paleozoic amalgamation of Eurasia. Tectonophysics 455, 61–76.

Alekseev, D.V., Aristov, V.A., Degtyarev, K.E., 2007. The age and tectonic setting of volcanic and cherty sequences in the ophiolite complex of the Atbashe Ridge (Southern Tien Shan). Doklady Earth Sciences 413, 380–383.

Alekseev, D.V., Degtyarev, E.V., Kotov, A.B., Sal'nikova, E.B., Tret'yakov, A.A., Yakovleva, S.Z., Anisimova, I.V., Shatagin, K.N., 2009. Late Paleozoic subductional and collisional igneous complexes in the Naryn segment of the Middle Tien Shan (Kyrgyzstan). Doklady Earth Sciences 42, 760–763.

Alexeiev, D.V., Cook, H.E., Buvtyshkin, V.M., Golub, L.Y., 2009. Structural evolution of the Ural–Tian Shan junction: a view from Karatau ridge, South Kazakhstan. Comptes Rendus Geoscience 341, 287–297.

Allen, M.B., Vincent, S.J., 1997. Fault reactivation in the Junggar region, northwest China: the role of basement structures during Mesozoic–Cenozoic compression. Journal of the Geological Society of London 154, 151–155.

Allen, M.B., Alsop, G.I., Zhemchuzhnikov, V.G., 2001. Dome and basin refolding and transpressive inversion along the Karatau fault system, southern Kazakhstan. Journal of the Geological Society of London 158, 83–95.

Bazhenov, M.L., Mikolaichuk, A.V., 2002. Paleomagnetism of Paleogene basalts from the Tien Shan, Kyrgyzstan: rigid Eurasia and dipole geomagnetic field. Earth and Planetary Science Letters 195, 155–166.

Biske, Yu.S., Seltmann, R., 2010. Paleozoic Tian-Shan as a transitional region between the Rheic and Urals–Turkestan oceans. Gondwana Research 17, 602–613.

Bullen, M.E., Burbank, D.W., Garver, J.I., Abdrakhmatov, K.Y., 2001. Late Cenozoic tectonic evolution of the northwestern Tien Shan: new age estimates for the initiation of mountain building. Geological Society of America Bulletin 113, 1544–1559.

Bullen, M.E., Burbank, D.W., Garver, J.I., 2003. Building the northern Tien Shan: integrated thermal, structural and topographic constraints. Journal of Geology 111, 149–165.

Burtman, 2010. Tien Shan, Pamir, and Tibet: history and geodynamics of Phanerozoic oceanic basins. Geotectonics 44, 388–404.

Buslov, M.M., Klerkx, J., Abdrakhmatov, K., Delvaux, D., Batalev, V.Y., Kuchai, O.A., Dehandschutter, B., Muraliev, A., 2003a. Recent strike-slip deformation of the northern Tien Shan. In: Storti, F., Holdsworth, R.E., Salvini, F. (Eds.), Intraplate Strike-slip Deformation Belts: Geological Society, London, Special Publication, 210, pp. 53–64.

Buslov, M., Watanabe, T., Smirnova, L., Fujiwara, I., Iwata, K., De Grave, J., Semakov, N., Travin, A., Kiryanova, A., Kokh, D., 2003b. Role of strike-slip faults in Late Paleozoic–Early Mesozoic tectonics and geodynamics of the Altai-Sayan and East Kazakhstan folded zone. Russian Geology and Geophysics 44, 49–75.

Buslov, M.M., De Grave, J., Bataleva, E.A., Batalev, V.Y., 2007. Cenozoic tectonic and geodynamic evolution of the Kyrgyz Tien Shan Mountains: synthesis of geological, thermochronological and geophysical data. Journal of Asian Earth Sciences 29, 205–214.

Charreau, J., Gumiaux, C., Avouac, J.-P., Augier, R., Chen, Y., Barrier, L., Gilder, S., Dominguez, S., Charles, N., Wang, Q., 2009. The Neogene Xiyu Formation, a diachronous prograding gravel wedge at front of the Tianshan: climatic and tectonic implications. Earth and Planetary Science Letters 287, 298–310.

Chen, C., Lu, H., Jia, D., Cai, D., Wu, S., 1999. Closing history of the southern Tianshan oceanic basin, western China: an oblique collisional orogeny. Tectonophysics 302, 23–40.

Chen, X., Shu, L., Santosh, M., 2011. Late Paleozoic post-collisional magmatism in the Eastern Tianshan Belt, Northwest China: new insights from geochemistry, geochronology and petrology of bimodal volcanic rocks. Lithos 127, 581–598.

Cherniak, D.J., Watson, E.B., 2003. Diffusion in zircon. Reviews in Mineralogy and Geochemistry 53, 113–143.

Cobbold, P.R., Sadybakasov, E., Thomas, J.C., 1994. Cenozoic transpression and basin development, Kyrghyz Tienshan, Central Asia. In: Roure, F., Ellouz, N., Shein, V.S., Skvortsov, I. (Eds.), Geodynamic Evolution of Sedimentary Basins. International Symposium, Moscow, pp. 181–202.

Cogné, J.P., Kravchinsky, V.A., Halim, N., Hankard, F., 2005. Late Jurassic–Early Cretaceous closure of the Mongol–Okhotsk Ocean demonstrated by new Mesozoic paleomagnetic results from the Trans-Baikal area (SE Siberia). Geophysical Journal International 163, 813–832.

Coyle, D.A., Wagner, G.A., 1998. Positioning the titanite fission-track partial annealing zone. Chemical Geology 149, 117–125.

De Batist, M., Imbo, Y., Vermeesch, P., Klerkx, J., Giralt, S., Delvaux, D., Lignier, V., Beck, C., Kalugin, I., Abdrakhmatov, K.E., 2002. Bathymetry and sedimentary environments of Lake Issyk-Kul, Kyrgyz Republic (Central Asia): a large, high-altitude, tectonic lake. In: Klerkx, J., Imanackunov, B. (Eds.), Lake Issyk-Kul: Its Natural Environment. Kluwer Academic Publishers, Dordrecht, pp. 101–123.

De Grave, J., Van den haute, P., 2002. Denudation and cooling of the Lake Teletskoye region in the Altai Mountains (South Siberia) as revealed by apatite fission-track thermochronology. Tectonophysics 349, 145–159.

De Grave, J., Buslov, M.M., Zhimulev, F., Vermeesch, P., McWilliams, M.O., Metcalf, J., 2006. The Early Ordovician age of deformations in the Kokchetav subduction–collision belt: new $^{40}Ar/^{39}Ar$ data. Russian Geology and Geophysics 47, 445–454.

De Grave, J., Buslov, M.M., Van den haute, P., 2007. Distant effects of India–Eurasia convergence and Mesozoic intracontinental deformation in Central Asia: constraints from apatite fission-track thermochronology. Journal of Asian Earth Sciences 29, 188–204.

De Grave, J., Van den haute, P., Buslov, M.M., Dehandschutter, B., Glorie, S., 2008. Apatite fission-track thermochronology applied to the Chulyshman Plateau, Siberian Altai Region. Radiation Measurements 43, 38–42.

De Grave, J., Buslov, M.M., Van den haute, P., Metcalf, J., Dehandschutter, B., McWilliams, M.O., 2009. Multi-Method chronometry of the Teletskoye graben and its basement, Siberian Altai Mountains: new insights on its thermo-tectonic evolution. The Geological Society of London Special Publication 324, 237–259.

De Grave, J., Glorie, S., Buslov, M.M., Izmer, A., Fournier-Carrie, A., Elburg, M., Batalev, V.Yu., Vanhaeke, F., Van den haute, P., 2011a. The thermo-tectonic history of the Song-Kul Plateau, Kyrgyz Tien Shan: constraints by apatite and titanite thermo-chronometry and zircon U/Pb dating. Gondwana Research 20, 745–763.

De Grave, J., Glorie, S., Zhimulev, F.I., Buslov, M.M., Elburg, M., Vanhaecke, F., Van den haute, P., 2011b. Emplacement and exhumation of the Kuznetsk–Alatau basement (Siberia): implications for the tectonic evolution of the Central Asian Orogenic Belt and sediment supply to the Kuznetsk, Minusa and West Siberian Basins. Terra Nova 23, 248–256.

De Grave, J., Glorie, S., Ryabinin, A., Izmer, A., Zhimulev, F., Buslov, M.M., Van den haute, P., Stockli, D.F., Batalev, V.Yu., Vanhaeke, F., Elburg, M., 2011c. Late Palaeozoic and Meso-

Cenozoic tectonic evolution of the Southern Kyrgyz Tien Shan: constraints from multi-method thermochronology in the Trans-Alai, Turkestan-Alai Section and the South-eastern Ferghana Basin. Journal of Asian Earth Sciences 44, 149–168.
Donelick, R.A., O'Sullivan, P.B., Ketcham, R.A., 2005. Apatite fission-track analysis. Reviews in Mineralogy and Geochemistry 58, 49–94.
Dong, Y., Zhang, G., Neubauer, F., Liu, X., Hauzenberger, C., Zhou, D., Li, W., 2011. Syn- and post-collisional granitoids in the Central Tianshan orogen: geochemistry, geochronology and implications for tectonic evolution. Gondwana Research 20, 568–581.
Dumitru, T.A., Zhou, D., Chang, E.Z., Graham, S.A., 2001. Uplift, exhumation, and deformation in the Chinese Tian Shan. Geological Society of America Memoir 194, 71–99.
Ehlers, T.A., Farley, K.A., 2003. Apatite (U–Th)/He thermochronometry: methods and applications to problems in tectonic and surface processes. Earth and Planetary Science Letters 206, 1–14.
Farley, K.A., 2002. (U–Th)/He dating: techniques, calibrations, and applications. Noble Gas Geochemistry: Reviews in Mineralogy and Geochemistry, 47, pp. 819–844.
Flowers, R.M., Kelley, S.A., 2011. Interpreting data dispersion and "inverted" dates in apatite (U–Th)/He and fission-track datasets: an example from the US midcontinent. Geochemica and Cosmochemica Acta 75, 5169–5186.
Gao, J., Lingli, L., Klemd, R., Qian, Q., Liu, D., Xiong, X., Su, W., Liu, W., Wang, Y., Yang, F., 2009. Tectonic evolution of the South Tianshan orogen and adjacent regions, NW China: geochemical and age constraints of granitoid rocks. International Journal of Earth Sciences 98 (6), 1221–1238.
Glorie, S., De Grave, J., Buslov, M.M., Elburg, M.A., Stockli, D.F., Van den haute, P., Gerdes, A., 2010. Multi-method chronometric constraints on the evolution of the Northern Kyrgyz Tien Shan batholith: from emplacement to exhumation. Journal of Asian Earth Sciences 38, 131–146.
Glorie, S., De Grave, J., Buslov, M.M., Zhimulev, F.I., Izmer, A., Vandoorne, W., Ryabinin, A., Van den haute, P., Vanhaecke, F., Elburg, M., 2011a. Formation and Palaeozoic evolution of the Gorny-Altai–Altai-Mongolia suture zone (South Siberia): ziron U/Pb constraints on its igneous record. Gondwana Research 20, 465–484.
Glorie, S., De Grave, J., Buslov, M.M., Zhimulev, F.I., Stockli, D.F., Batalev, V.Yu, Izmer, A., Van den haute, P., Vanhaecke, F., Elburg, M.A., 2011b. Thermotectonic history of the Kyrgyz South Tien Shan (Atbashi–Inylchek) suture zone: the role of inherited structures during deformation–propagation. Tectonics 30, TC6016. http://dx.doi.org/10.1029/2011TC002949 (23 pp.).
Glorie, S., De Grave, J., Delvaux, D., Van den haute, P., Buslov, M.M., 2012. Tectonic history of the Irtysh shear zone (Rudny Altai, Kazakhstan): new constraints from zircon U/Pb dating, apatite fission track dating and paleostress analysis. Journal of Asian Earth Sciences 45, 138–149.
Golonka, J., 2004. Plate tectonic evolution of the southern margin of Eurasia in the Mesozoic and Cenozoic. Tectonophysics 381, 235–273.
Graham, S.A., Hendrix, M.S., Wang, L.B., Carroll, A.R., 1993. Collisional successor basins of western China: impact of tectonic inheritance on sand composition. Geological Society of America Bulletin 105, 323–344.
Green, P.F., Duddy, I.R., 2006. Interpretation of apatite (U–Th)/He ages and fission track ages from cratons. Earth and Planetary Science Letters 244, 541–547.
Han, B.-F., He, G.-Q., Wang, X.-C., Guo, Z.-J., 2011. Late Carboniferous collision between the Tarim and Kazakhstan–Yili terranes in the western segment of the South Tian Shan Orogen, Central Asia, and implications for the Northern Xinjiang, western China. Earth-Science Reviews 109, 74–93.
Hendrix, M.S., 2000. Evolution of Mesozoic sandstone compositions, southern Junggar, northern Tarim, and western Turpan basins, northwest China: a detrital record of the ancestral Tian Shan. Journal of Sedimentary Research 70, 520–532.
Hendrix, M.S., Dumitru, T.A., Graham, S.A., 1994. Late Oligocene–Early Miocene unroofing in the Chinese Tien Shan: an early effect of the India–Asia collision. Geology 22, 487–490.
Hoskin, P.W.O., Schaltegger, U., 2003. The composition of zircon and igneous and metamorphic petrogenesis. Reviews in Mineralogy and Geochemistry 53, 27–62.
Jenchuraeva, R., Bakirov, A., Ghes, M., Seltmann, R., Shatov, V., Popov, V., 2001. Mineral Deposits Map of Kyrgyzstan, 1:1,000,000. International Association on the Genesis of Ore Deposits, London-Bishkek.
Ji, J., Luo, P., White, P., Jiang, H., Gao, L., Ding, Z., 2008. Episodic uplift of the Tianshan Mountains since the late Oligocene constrained by magnetostratigraphy of the Jingou River section, in the southern margin of the Junggar Basin, China. Journal of Geophysical Research 113, B05102 (14 pp.).
Jolivet, M., Ritz, J.-F., Vassallo, R., Larroque, C., Braucher, R., Todbileg, M., Chauvet, A., Sue, C., Arnaud, N., De Vicente, R., Arzhanikova, A., Arzhanikov, S., 2007. Mongolian summits: an uplifted, flat, old but still preserved erosion surface. Geology 35, 871–874.
Jolivet, M., De Boisgrollier, T., Petit, C., Fournier, M., Sankov, V.A., Ringenbach, J.-C., Byzov, L., Miroshnichenko, A.I., Kovalenko, S.N., Anisimova, S.V., 2009. How old is the Baikal Rift Zone? Insights from apatite fission track thermochronology. Tectonics 28, TC3008. http://dx.doi.org/10.1029/2008TC002404.
Jolivet, M., Dominguez, S., Charreau, J., Chen, Y., Li, Y.G., Wang, Q.C., 2010. Mesozoic and Cenozoic tectonic history of the central Chinese Tian Shan: reactivated tectonic structures and active deformation. Tectonics 29, TC6019. http://dx.doi.org/10.1029/2010TC002712.
Kapp, P., DeCelles, P.G., Gehrels, G.E., Heizler, M., Ding, L., 2007. Geological records of the Lhasa–Qiangtang and Indo-Asian collisions in the Nima area of central Tibet. Geological Society of America Bulletin 119, 917–932.
Ketcham, R.A., 2005. Forward and inverse modeling of low-temperature thermochronometry data. Reviews in Mineralogy and Geochemistry 58, 275–314.
Ketcham, R.A., Donelick, R.A., Carlson, W.D., 1999. Variability of apatite fission-track annealing kinetics: III. Extrapolation to geologic time scales. American Mineralogist 84, 1235–1255.
Khain, E.V., Bibikova, E.V., Salnikova, E.B., Kröner, A., Gibsher, A.S., Didenko, A.N., Degtyarev, K.E., Fedotova, A.A., 2003. The Palaeo-Asian Ocean in the Neoproterozoic and early Palaeozoic: new geochronologic data and palaeotectonic reconstructions. Precambrian Research 122, 329–358.
Kohn, B.P., Wagner, M.E., Lutz, T.M., Organist, G., 1993. Anomalous Mesozoic thermal regime, Central Appalachian–Piedmont — evidence from sphene and zircon fission-track dating. Journal of Geology 101, 779–794.
Konopelko, D., Biske, G., Seltmann, R., Eklund, O., Belyatsky, B., 2007. Hercynian post-collisional A-type granites of the Kokshaal Range, Southern Tien Shan, Kyrgyzstan. Lithos 97, 140–160.
Konopelko, D., Biske, G., Seltmann, R., Kiseleva, M., Matukov, D., Sergeev, S., 2008. Deciphering Caledonian events: timing and geochemistry of the Caledonian magmatic arc in the Kyrgyz Tien Shan. Journal of Asian Earth Sciences 32, 131–141.
Konopelko, D., Seltmann, R., Biske, G., Lepekhina, E., Sergeev, S., 2009. Possible source dichotomy of contemporaneous post-collision barren I-type versus tin-bearing A-type granites, lying on opposite sides of the South Tien Shan suture. Ore Geology Reviews 35, 206–216.
Kröner, A., Alexeiev, D.V., Mikolaichuk, A., Xia, X., Zack, T., Windley, B.F., Sun, M., Rojas-Agramonte, Y., Liu, D., 2009. New single zircon ages of Precambrian and Palaeozoic rocks from the Northern, Middle and Southern Tianshan belts in Kyrgyzstan. Abstract, International Excursion and Workshop on Tectonic Evolution and Crustal Structure of the Tien Shan Belt and Related Terrains in the Central Asian Orogenic Belt, Bishkek, 9–17 June 2009, p. 30.
Kröner, A., Alexeiev, D.V., Hegner, E., Rojas-Agramonte, Y., Corsini, M., Chao, Y., Wong, J., Windley, B.F., Liu, D., Tretyakov, A.A., 2012. Zircon and muscovite ages, geochemistry, and Nd–Hf isotopes for the Aktyuz metamorphic terrane: evidence for an Early Ordovician collisional belt in the northern Tianshan of Kyrgyzstan. Gondwana Research. 21, 901–927.
Leier, A.L., DeCelles, P.G., Kapp, P., Gehrels, G.E., 2007. Lower Cretaceous strata in the Lhasa terrane, Tibet, with implications for understanding the early tectonic history of the Tibetan Plateau. Journal of Sedimentary Research 77, 809–825.
Leloup, P.H., Boutonnet, E., Davis, W.J., Hattori, K., 2011. Long-lasting intracontinental strike-slip faulting: new evidence from the Karakorum shear zone in the Himalayas. Terra Nova 23, 92–99.
Li, C., Dupont-Nivet, G., Guo, Z., 2011a. Magnetostratigraphy of the Northern Tian Shan foreland, Taxi He section, China. Basin Research 23, 101–117.
Li, Z., Chen, H., Song, B., Li, Y., Yang, S., Yu, X., 2011b. Temporal evolution of the Permian large igneous province in Tarim Basin in northwestern China. Journal of Asian Earth Sciences 42, 917–927.
Ludwig, K., 2003. User's Manual for Isoplot 3.00, A Geochronological Toolkit for Microsoft Excel. Berkeley Geochronology Center Special Publication v. 4.
McDougall, I., Harrison, M., 1999. Geochronology and Thermochronology by the $^{40}Ar/^{39}Ar$ Method. Oxford University Press. 269 pp.
Metelkin, D.V., Vernikovsky, V.A., Kazansky, A.Y., Wingate, M.T.D., 2010. Late Mesozoic tectonics of Central Asia based on paleomagnetic evidence. Gondwana Research 18, 400–419.
Mikolaichuk, A.V., 2000. The structural position of thrusts in the recent orogen of the central Tien Shan. Russian Geology and Geophysics 41, 929–939.
Mikolaichuk, A.V., Kurenkov, S.A., Degtyarev, K.E., Rubtsov, V.I., 1997. Northern Tien Shan main stages of geodynamic evolution. Geotectonics 31, 445–462.
Mikolaichuk, A.V., Gubrenko, M.V., Bogomolov, L.M., 2003. Fold deformations of a preorogenic peneplain in the recent structure of the central Tien Shan. Geotectonics 37, 31–37.
Molnar, P., Tapponnier, P., 1975. Cenozoic tectonics of Asia: Effects of a continental collision. Science 189, 419–426.
Otto, S.C., 1997. Mesozoic–Cenozoic history of deformation and petroleum systems in sedimentary basins of Central Asia: implications of collisions on the Eurasian margin. Petroleum Geoscience 3, 327–341.
Pirajno, F., 2010. Intracontinental strike-slip faults, associated magmatism, mineral systems and mantle dynamics: examples from NW China and Altay–Sayan (Siberia). Journal of Geodynamics 50, 325–346.
Poupinet, G., Avouac, J.-P.h., Jiang, M., Wei, S., Kissling, E., Herquel, G., Guilbert, J., Paul, A., Wittlinger, G., Su, H., Thomas, J.-C., 2002. Intracontinental subduction and Palaeozoic inheritance of the lithosphere suggested by a teleseismic experiment across the Chinese Tien Shan. Terra Nova 14, 18–24.
Pullen, A., Kapp, P., Gehrels, G.E., Vervoort, J.D., Ding, L., 2008. Continental subduction in central Tibet and Mediterranean-style closure of the Paleo-Tethys Ocean. Geology 36, 351–354.
Qin, K.-Z., Su, B.-X., Asamoah Sakyi, P., Tang, D.-M., Li, X.-H., Sun, H., Xiao, Q.-H., Liu, P.-P., 2011. SIMS zircon U–Pb geochronology and Sr–Nd isotopes of Ni–Cu-bearing mafic–ultramafic intrusions in eastern Tianshan and Beishan in correlation with flood basalts in Tarim Basin (NW China): constraints on a ca. 280 Ma mantle plume. American Journal of Science 311, 237–260.
Ratschbacher, L., Hacker, B.R., Webb, L.E., Grimmer, J.C., McWilliams, M.O., Ireland, T., Dong, S., Hu, J.-M., 2003. Tectonics of the Qinling (Central China): tectonostratigraphy, geochronology, and deformation history. Tectonophysics 366, 1–53.
Reiners, P.W., Spell, T.L., Nicolescu, S., Zanetti, K.A., 2004. Zircon (U–Th)/He thermochronometry: He diffusion and comparisons with Ar-40/Ar-39 dating. Geochimica et Cosmochimica Acta 68, 1857–1887.
Schmidt, J., Hacker, B.R., Ratschbacher, L., Stübner, K., Stearns, M., Kylander-Clark, A., Cottle, J.M., Alexander, A., Webb, G., Gehrels, G., Minaev, V., 2011. Cenozoic deep crust in the Pamir. Earth and Planetary Science Letters 312, 411–421.
Schwab, M., Ratschbacher, L., Siebel, W., McWilliams, M., Minaev, V., Lutkov, V., Chen, F., Stanek, K., Nelson, B., Frisch, F., Wooden, J.L., 2004. Assembly of the Pamirs: age and origin of magmatic belts from the southern Tien Shan to the southern Pamirs and their relation to Tibet. Tectonics 23, TC4002. http://dx.doi.org/10.1029/2003TC001583 (31 pp.).

Seltmann, R., Konopelko, D., Biske, G., Divaev, F., Sergeev, S., 2011. Hercynian post-collisional magmatism in the context of Paleozoic magmatic evolution of the Tien Shan orogenic belt. Journal of Asian Earth Sciences 42, 821–838.
Shuster, D.L., Flowers, R.M., Farley, K.A., 2006. The influence of natural radiation damage on helium diffusion kinetics in apatite. Earth and Planetary Science Letters 249, 148–161.
Sobel, E.R., Dumitru, T.A., 1997. Thrusting and exhumation around the margins of the western Tarim Basin during the India–Asia collision. Journal of Geophysical Research 102, 5043–5064.
Sobel, E., Chen, J., Heermance, R.V., 2006a. Late Oligocene–Early Miocene initiation of shortening in the SW Chinese Tian Shan: implications for Neogene shortening rate variations. Earth and Planetary Science Letters 247, 70–81.
Sobel, E.R., Oskin, M., Burbank, D., Mikolaichuk, A., 2006b. Exhumation of basement cored uplifts: example of the Kyrgyz Range quantified with apatite fission track thermochronology. Tectonics 25, TC2008. http://dx.doi.org/10.1029/2005TC001809.
Spiegel, C., Kohn, B., Belton, D., Berner, Z., Gleadow, A., 2009. Apatite (U–Th–Sm)/He thermochronology of rapidly cooled samples: the effect of He implantation. Earth and Planetary Science Letters 285, 105–114.
Sun, J., Xu, Q., Huang, B., 2007. Late Cenozoic magnetochronology and paleoenvironmental changes in the northern foreland basin of the Tian Shan Mountains. Journal of Geophysical Research 112, B04107 (14 pp.).
Thompson, S., Weldon, R.J., Rubin, C.M., Abdrakhmatov, K., Molnar, P., Berger, G.W., 2002. Late Quaternary slip rates across the central Tien Shan, Kyrgyzstan. Journal of Geophysical Research 107 (B9), 2203.
Tian, W., Campbell, I.H., Allen, C.M., Guan, P., Pan, W., Chen, M., Yu, H., Zhu, W., 2010. The Tarim picrite–basalt–rhyolite suite, a Permian flood basalt from northwest China with contrasting rhyolites produced by fractional crystallization and anatexis. Contributions to Mineralogy and Petrology 160, 407–425.
Tursungaziev, B.T., Petrov, O.B., 2008. Geological map of the Kyrgyz Republic, 1:500,000. Agency of Geology and Mineralogical Resources of the Kyrgyz Republic, Bishkek.
Van der Voo, R., Levashova, N.M., Skrinnik, L.I., Kara, T.V., Bazhenov, M.L., 2006. Late orogenic, large-scale rotations in the Tien Shan and adjacent mobile belts in Kyrgyzstan and Kazakhstan. Tectonophysics 426, 335–360.
Vassallo, R., Jolivet, M., Ritz, J.-F., Brauchner, R., Larroque, C., Sue, C., Todbileg, M., Javkhlanbold, D., 2007. Uplift age and rates of the Gurvan Bogd system (Gobi–Altay) by apatite fission track analysis. Earth and Planetary Science Letters 259, 333–346.
Wagner, G.A., Van den haute, P., 1992. Fission Track-Dating. Kluwer Academic Publishers, Dordrecht, the Netherlands. 285 pp.
Wang, Q.C., Li, S.J., Du, Z.L., 2009. Differential uplift of the Chinese Tianshan since the Cretaceous: constraints from sedimentary petrography and apatite fission-track dating. International Journal of Earth Sciences 98, 1341–1363.
Wang, Q., Li, Z.-X., Chung, S.-L., Wyman, D.A., Sun, Y.-L., Zhao, Z.-H., Zhu, Y.-T., Qiu, H.-N., 2011. Late Triassic high-Mg andesite/dacite suites from northern Hohxil, North Tibet: geochronology, geochemical characteristics, petrogenetic processes and tectonic implications. Lithos 126, 54–67.
Wang, B., Jahn, B.M., Shu, L., Li, K., Chung, S.L., Liu, D., 2012. Middle–Late Ordovician arc-type plutonism in the NW Chinese Tianshan: implication for the accretion of the Kazakhstan continent in Central Asia. Journal of Asian Earth Sciences 49, 40–53.
Wilde, A.R., Layer, P., Mernagh, T., Foster, J., 2001. The giant Muruntau gold deposit: geologic, geochronologic, and fluid inclusion constraints on ore genesis. Economic Geology 96, 633–644.
Windley, B.F., Alexeiev, D., Xiao, W., Kröner, A., Badarch, G., 2007. Tectonic models for accretion of the Central Asian Orogenic Belt. Journal of the Geological Society of London 164, 31–47.
Wolf, R.A., Farley, K.A., Silver, L.T., 1996. Helium diffusion and low temperature thermochronometry of apatite. Geochimica et Cosmochimica Acta 60, 4231–4240.
Wolfe, M.R., Stockli, D.F., 2010. Zircon (U–Th)/He thermochronometry in the KTB drill hole, Germany, and its implications for bulk He diffusion kinetics in zircon. Earth and Planetary Science Letters 295, 69–82.
Xiao, W.J., Huang, B.C., Han, C.M., Sun, S., Li, J.L., 2010. A review of the western part of the Altaids: a key to understanding the architecture of accretionary orogens. Gondwana Research 18, 253–273.
Yang, S.H., Zhou, M.F., 2009. Geochemistry of the 430-Ma Jingbulake mafic–ultramafic intrusion in Western Xinjiang, NW China: implications for subduction related magmatism in the South Tianshan orogenic belt. Lithos 113, 259–273.
Zhai, Q.-G., Jahn, B.-M., Zhang, R.-Y., Wang, J., Su, L., 2011. Triassic subduction of the Paleo-Tethys in northern Tibet, China: evidence from the geochemical and isotopic characteristics of eclogites and blueschists of the Qiangtang block. Journal of Asian Earth Sciences 42, 1356–1370.
Zhang, C.-L., Li, Z.-X., Li, X.-H., Ye, H.-M., Li, C.-N., 2008. A Permian layered intrusive complex in the western Tarim Block, NW China: product of a ca. 275 Ma mantle plume? Journal of Geology 116, 269–287.
Zhang, Z., Zhu, W., Shu, L., Wan, J., Yang, W., Su, J., Zheng, B., 2009. Apatite fission track thermochronology of the Precambrian Aksu blueshist, NW China: implications for the thermo-tectonic evolution of the north Tarim basement. Gondwana Research 16, 182–188.
Zhang, C.-L., Li, Z.-X., Li, X.-H., Xu, Y.-G., Zhou, G., Ye, H.-M., 2010a. A Permian large igneous province in Tarim and Central Asian orogenic belt, NW China: results of a ca. 275 Ma mantle plume? Geological Society of America Bulletin 122, 2020–2040.
Zhang, Y., Liu, J., Guo, Z., 2010b. Permian basaltic rocks in the Tarim basin, NW China: implications for plume–lithosphere interaction. Gondwana Research 18, 596–610.
Zhang, Z., Zhu, W., Shu, L., Wan, J., Yang, W., Zheng, B., Su, J., 2011. Multi-stage exhumation of the NE Tarim Precambrian bedrock, NW China: constraints from apatite fission track thermochronology in the Kuluketage area. Terra Nova 23, 324–332.
Zhimulev, F.I., Buslov, M.M., Travin, A.V., Dmitrieva, N.V., De Grave, J., 2011. Early–Middle Ordovician nappe tectonics of the junction between the Kokchetav HP–UHP metamorphic belt and the Stepnyak paleoisland arc (northern Kazakhstan). Russian Geology and Geophysics 52, 109–123.